

Table D1.2-7. Failure Probabilities for the DOE Spent Nuclear Fuel (DSNF) Canisters and Multicanister Overpack (MCO)

Component	Peak Equivalent Plastic Strain (%)			Probability of Failure					
				Original CDF			CDF adjusted to min elongation		
	Outside Surface	Middle	Inside Surface	Outside Surface	Middle	Inside Surface	Outside Surface	Middle	Inside Surface
<b>18-inch standard canister containment PEEQ strains, 3 degrees off vertical drop, 300°F</b>									
Lower head	8	3	6	<1E-08	<1E-08	<1E-08	<1E-08	<1E-08	<1E-08
Lower head-to-main shell weld	2	2	3	<1E-08	<1E-08	<1E-08	<1E-08	<1E-08	<1E-08
Main shell	2	2	3	<1E-08	<1E-08	<1E-08	<1E-08	<1E-08	<1E-08
Upper head-to-main shell weld	0	0	0	<1E-08	<1E-08	<1E-08	<1E-08	<1E-08	<1E-08
Upper head	1	0.2	2	<1E-08	<1E-08	<1E-08	<1E-08	<1E-08	<1E-08
<b>24-inch standard canister containment PEEQ strains, 3 degrees off vertical drop, 300°F</b>									
Lower head	2	0.7	1	<1E-08	<1E-08	<1E-08	<1E-08	<1E-08	<1E-08
Lower head-to-main shell weld	0.2	0.3	0.5	<1E-08	<1E-08	<1E-08	<1E-08	<1E-08	<1E-08
Main shell	0.2	0.3	0.5	<1E-08	<1E-08	<1E-08	<1E-08	<1E-08	<1E-08
Upper head-to-main shell weld	0	0	0	<1E-08	<1E-08	<1E-08	<1E-08	<1E-08	<1E-08
Upper head	0	0	0	<1E-08	<1E-08	<1E-08	<1E-08	<1E-08	<1E-08
<b>4 MCO containment PEEQ strains, 3 degrees off vertical drop, 70°F</b>									
Bottom	35	16	14	3.74E-03	<1E-08	<1E-08	8.99E-02	<1E-08	<1E-08
Bottom-to-main shell	21	11	11	<1E-08	<1E-08	<1E-08	1.16E-07	<1E-08	<1E-08
Main shell	13	15	29	<1E-08	<1E-08	1.09E-06	<1E-08	<1E-08	3.85E-03
Collar	0	0	0	<1E-08	<1E-08	<1E-08	<1E-08	<1E-08	<1E-08
Cover	0	0	0	<1E-08	<1E-08	<1E-08	<1E-08	<1E-08	<1E-08

NOTE: ASME = The American Society of Mechanical Engineers; CDF = cumulative distribution function; DOE STD = U.S. Department of Energy standard; MCO = multicanister overpack; PEEQ = peak equivalent.

Source: Ref. D4.1.27, Tables 6.3.7.6-4 and 6.3.7.6-5

### D1.3 PROBABILITIES OF FAILURE OF HIGH-LEVEL WASTE CANISTERS DUE TO DROPS

The probability of failure for drops of HLW canisters was assessed by evaluating actual drop test data. Several series of tests were conducted including vertical, top, and corner drops of steel containers. The reports on these tests are summarized in *Leak Path Factors for Radionuclide Releases from Breached Confinement Barriers and Confinement Areas* (Ref. D4.1.17). No leaks were found after 27 tests, 14 of which were from 23 feet and 13 of which were from 30 feet. These tests can be interpreted as a series of Bernoulli trials, for which the outcome is the breach, or not, of the tested canister. The observation of zero failures in 13 tests was interpreted using a beta-binomial conjugate distribution Bayes analysis.

A uniform prior distribution, which indicates prior knowledge that the probability of failure is between 0 and 1, may be represented as a Beta(r,s) distribution in which both r and s equals 1. The conjugate pair likelihood function for a Beta(r,s) distribution is a Binomial(n, N) where n represents the number of failures within the tests and N represents the number of tests. The posterior distribution resulting from the conjugate pairing is also a Beta distribution with parameters r' and s', which are defined as follows:

$$r' = r + n \quad \text{and} \quad s' = s + N - n \quad (\text{Eq. D-1})$$

The mean,  $\mu$ , and standard deviation,  $\sigma$ , of the posterior distribution are determined using the following equations:

$$\mu = r' / (r' + s') \quad \text{and} \quad \sigma = \{r's' / [(r' + s' + 1)(r' + s')^2]\}^{1/2} \quad (\text{Eq. D-2})$$

For n = 0 and N = 13, Equation D-2 results in  $\mu = 0.067$  and  $\sigma = 0.062$ . For n = 0 and N = 27,  $\mu = 0.034$  and  $\sigma = 0.033$ . These values are used for the failure probability of a dropped HLW canister, for example during its transfer by a canister transfer machine.

One element of the Nuclear Safety Design Basis (Section 6.9) requires that the transportation cask, which will deliver HLW and DOE standardized canisters, be designed to preclude contact between the canister and a transportation cask lid or other heavy object that might fall. Similarly, other large heavy objects are precluded from damaging these canisters, when residing within a co-disposal waste package by the design of the waste package, which includes separator plates that extend well above the canisters. These scenarios are not quantitatively analyzed herein.

The combined INL and LLNL analyses discussed previously conclude that a DOE SNF canister has a probability of breach less than 1E-08 for a 23-foot drop, 4 degrees off-normal (i.e., 4 degrees from vertical) onto an unyielding rigid surface. The LLNL results demonstrate that generally strains from impact and probability of failure is higher for off-normal drops than normal (i.e., vertical) drops for the same height. The LLNL results further show that a 10-ton load dropped from 10 feet onto a representative canister also results in a probability of breach of less than 1E-08. *Qualitative Analysis of the Standardized DOE SNF Canister for Specific Canister-on-Canister Drop Events at the Repository* (Ref. D4.1.67) states that canister integrity was maintained for a 30-foot drop test onto a rigid, unyielding surface. The report discusses

drop of a HLW canister on a DOE SNF canister and drop of a DOE SNF canister onto another one. Drops of these canisters onto canisters in the Initial Handling Facility or Canister Receipt and Closure Facility (CRCF) would occur with drop heights of less than 10 feet. Two main differences are noted between a drop of a DOE SNF and a drop of a HLW canister onto a DOE SNF. The first is that substantially lower kinetic energy of impact of the latter drop would result in significantly less skirt deformation. The non-flat bottom nature of the HLW/DOE SNF interaction would have a different skirt deformation pattern than the flat bottomed drop. INL concludes that the skirt would be expected to absorb the bulk of the heaviest HLW canister (4.6 tons) drop energy and DOE SNF canister integrity would be maintained. A difference between a 10-ton drop of a load onto a representative canister and a drop onto a DOE SNF canister results from the difference diameters of the target as well as different materials and lid thicknesses. Nevertheless, INL concludes that the impact from 10 feet of a HLW canister onto a DOE SNF canister is less challenging than impact from a 30-foot drop. Since the probability from a 23-foot drop was calculated to be less than 1E-08, it is conservative to use a value of 1E-05 for the probability of failure of an HLW on DOE SNF impact. The increased value is assigned to account for uncertainties owing to the differences noted above.

#### **D1.4 PROBABILITIES OF FAILURE OF WASTE PACKAGES DUE TO DROPS AND IMPACTS**

The probabilities of containment failure are evaluated by comparing the challenge load with the capacity of the waste package to withstand that challenge in a manner similar to that described in HLWRS-ISG-02 (Ref. D4.1.56), and summarized in Section 4.3.2.2. Three scenarios are evaluated for the potential loss of containment by waste packages due to drops and impacts:

- Two-foot horizontal drop
- 3.4 mph end-to-end impact
- Rockfall on waste package in subsurface tunnels.

An additional scenario, drop of a waste package shield ring onto a waste package, is considered in Section D1.4.4.

For this assessment, the potential load has been determined by FEA in the calculations cited below as the sources of inputs. The load is expressed in terms of stress intensities and as expended toughness fraction (ETF), which is the ratio of the stress intensity to the true tensile strength. The ETF is used to obtain the failure probability by the following:

$$P = \int_{-\infty}^x N(t) dt \quad \text{and} \quad x = \frac{ETF - 1}{COV} \quad (\text{Eq. D-3})$$

where

$P$	=	probability of failure
$N(t)$	=	standard normal distribution with mean of zero and standard deviation of one
$t$	=	variable of integration
$ETF$	=	expended toughness fraction
$COV$	=	coefficient of variation = ratio of standard deviation to mean for strain capacity distribution, applied here to stress capacity or true tensile strength

The capacity is the true tensile strength of the material, the stress the material can withstand before it separates. The minimum true tensile strength,  $\sigma_u$ , for the Alloy 22 typically used for the outer corrosion barrier (OCB) of the waste package is 971 MPa (Ref. D4.1.20, Section 7.7, p. 162). The variability in the capacity is expressed as the standard deviation of a normal distribution that includes strength variation data and variability of the toughness index,  $I_T$ , computed without triaxiality adjustments (uniaxial test data). The standard deviation as percent of the mean of  $\sigma_u$  is 7.3% (Ref. D4.1.20, Section 7.6, p. 162). The distribution of elongations used for defining the fragility curve in the LLNL analysis was expressed as two normal distributions, the larger of which was with a mean of 59.3% elongation and a standard deviation of 4.22% elongation, or a coefficient of variation (COV) of 0.0712 (Ref. D4.1.27, Section 6.3.7.3). Thus the 0.073 reported for the OCB material is conservative compared with the LLNL data and is used for the COV in the expression above. The possibility of waste package weld defects is not explicitly considered in the analysis. However, as noted in Section D.1.4.5, weld defects are not expected to contribute significantly to the probability of waste package failure due to drops or other impacts.

#### D1.4.1 Waste Package Drop

A study investigating the structural response of the naval long waste package to a drop while it is being carried on the emplacement pallet, found the ETF for the OCB to be 0.29 for a 10 m/sec flat impact (Ref. D4.1.20, Table 7-15, pg. 117), equivalent to a 16.7-foot drop. This corresponds to a failure probability of less than  $1 \times 10^{-8}$ . The failure of the OCB is used to define the loss of containment, taking no credit for the inner vessel and the canister within. The description of the transport and emplacement vehicle (TEV) provided in *Mechanical Handling Design Report: Waste Package Transport and Emplacement Vehicle* (Ref. D4.1.12) mentions that the floor plate is lifted by four jacks and guided by a roller. The guide roller precludes tilted drops of the flat bed of the TEV. As was done for the results from LLNL, to introduce an additional measure of conservatism, a failure probability of  $1 \times 10^{-5}$  is used for the probability that the waste package containment would fail due to a two-foot horizontal drop, which is much less severe than the modeled 16.7-foot drop.

#### D1.4.2 Rockfall onto a Waste Package

A seismic event during the preclosure period could cause rocks to fall from the ceiling of a drift onto the waste packages stored there prior to deployment of the drip shields. The extent of

damage has been predicted for several levels of impact energy of falling rocks (Ref. D4.1.26). The maximum credible impact energy from a falling rock is about  $1 \times 10^6$  joules (J) (Ref. D4.1.21, p. 57). The maximum ETF resulting from rockfall impacting with approximately  $1 \times 10^6$  J is about 0.11 (Ref. D4.1.26, p. 54, Table 5), corresponding to a failure probability less than  $1 \times 10^{-8}$ . As was done for the results from LLNL, to introduce an additional measure of conservatism, a failure probability of  $1 \times 10^{-5}$  should be used for the probability that the waste package containment would fail due to rockfall on the waste package.

### D1.4.3 Results for the Three Assessed Scenarios

The failure probabilities for the three scenarios, derived from the results in the cited reports, are summarized in Table D1.4-1.

Table D1.4-1. Waste Package Probabilities of Failure for Various Drop and Impact Events

Event	Probability of Failure
2-Foot Horizontal Drop	$< 1 \times 10^{-5}$
3.4 mph end-to-end impact	$< 1 \times 10^{-5}$
20 metric ton rockfall on waste package with and without rock bolt <sup>a</sup> impacting the waste package	$< 1 \times 10^{-5}$

NOTE: <sup>a</sup>A rock bolt is a long anchor bolt, for stabilizing rock excavations, which may be tunnels or rock cuts.

Source: Original

### D1.4.4 Drop of a Waste Package Shield Ring onto a Waste Package

After the co-disposal waste package has been welded closed in the Waste Package Positioning Room, the shield ring is lifted from it before the waste package transfer trolley is moved into the load out area. Grapple failures might cause the drop to occur at a variety of orientations relative to the top of the waste package. A frequency of canister breach from a potential drop as high as 10 feet is considered here. For a canister breach to occur, the shield ring must penetrate the 1-inch thick outer lid made of SB 575 (Alloy 22) and the 9 inch thick stainless steel inner lid (SA 240) before having an opportunity to impact the canister (Ref. D4.1.13). There are six inches separating the inner and outer lids. In the radial center area of that space, which would be directly above the DOE SNF canister, is a stainless steel lifting device attached to the inner lid. This adds another layer of energy absorption.

The shield ring weighs approximately 15 tons and is made of stainless steel with a lighter weight neutron absorber material. The impact energy of a 15-ton shield ring dropping 10 feet would be 0.4 MJ. The frequency of penetration of the sides of a waste package from a 20 metric ton rock impacting the side of the waste package with impact energy of 1 MJ is less than  $1 \times 10^{-8}$  (Table D1.4-1). The sides of a waste package are approximately three inches thick compared to a cumulative thickness (excluding lifting fixture) of 10 inches at the top. Although the impact energy could be more focused, the impact energy for the shield ring against the top of the waste package is less than the impact energy of the rockfall against the side and the top is much thicker than the side. The probability of failure due to shield ring impact against the top of the waste

package is expected to be no worse than for the impact of a rock against the side. A conservative value of  $1 \times 10^{-5}$  is used in the analysis for this probability.

#### **D1.4.5 Waste Package Weld Defects**

Waste package closure involves engaging and welding the inner lid spread ring, inerting the waste package with helium, setting and welding the outer lid to the OCB, performing leak testing on the inner vessel closure, performing nondestructive examination of welds, and conducting postweld stress mitigation on the outer lid closure weld.

The weld process of the waste package closure subsystem is controlled as a special process by the Quality Assurance Program (Ref. D4.1.29, Section 9.0). The activities performed by the system are controlled by approved procedures.

The principal components of the system include welding equipment; nondestructive examination equipment for visual, eddy current, and ultrasonic inspections of the welds and leak detection; stress mitigation equipment for treatment of the outer lid weld; inerting equipment; and associated robotic arms. Other equipment includes the spread ring expander tool, leak detection tools, cameras, and the remote handling system. The system performs its functions through remote operation of the system components.

The capability of the waste package closure subsystem will be confirmed by demonstration testing of a full-scale prototype system. The prototype includes welding, nondestructive examinations, inerting, stress mitigation, material handling, and process controls subsystems. The objective of the waste package closure subsystem prototype program is to design, develop, and construct the complete system required to successfully close the waste package. An iterative process of revising and modifying the waste package closure subsystem prototype will be part of the design process. When prototype construction is finalized, a demonstration test of the closure operations will be performed on only the closure end of the waste package; thus, the mock-up will be full diameter but not full height as compared to the waste package. The purpose of the demonstration test is to verify that the individual subsystems and integrated system function in accordance with the design requirements and to establish closure operations procedures. This program is coordinated with the waste package prototype fabrication program.

The principal functions of the waste package closure subsystem are to:

- Perform a seal weld between the spread ring and the inner lid, the spread ring and the inner vessel, and the spread ring ends; perform a seal weld between the purge port cap and the inner lid; and perform a narrow groove weld between the outer lid and the OCB.
- Perform nondestructive examination of the welds to verify the integrity of the welds and repair any minor weld defects found.
- Purge and fill the waste package inner vessel with helium gas to inert the environment.
- Perform a leak detection test of the inner lid seals to ensure the integrity of the helium environment in the inner vessel.

- Perform stress mitigation of the outer lid groove closure weld to induce compressive residual stresses.

The gas tungsten arc welding process is used for waste package closure welds and weld repairs. Welding is performed in accordance with procedures qualified to the *2001 ASME Boiler and Pressure Vessel Code* (Ref. D4.1.5, Section IX), as noted below:

- The spread ring and purge port cap welds are two-pass seal welds.
- The outer lid weld is a multipass full-thickness groove weld.

Welding process procedures will be developed that identify the required welding parameters. The process procedures will:

- Identify the parameters necessary to consistently achieve acceptable welds.
- State the control method for each weld parameter and the acceptable range of values.

The welds are inspected in accordance with examination procedures developed using *2001 ASME Boiler and Pressure Vessel Code* (Ref. D4.1.5, Section V and Section III, Division 1, Subsection NC) as a guide, with modification as appropriate:

- Seal welds—visual inspection
- Groove welds—visual, eddy current, and ultrasonic inspection.

A weld dressing end effector is used for weld repairs. The defect is removed, resulting in an excavated cavity of a predetermined contour. The excavated cavity surface is inspected using the eddy current inspection end effectors. Then the cavity is welded and inspected in accordance with the welding and inspection procedures.

The stress mitigation process for the outer lid closure weld is controlled plasticity burnishing. Controlled plasticity burnishing is a patented method of controlled burnishing to develop specifically tailored compressive residual stress with associated controlled amounts of cold work at the outer surface of the waste package outer lid closure weld.

The inner vessel of the waste package is evacuated and backfilled with helium through a purge port on the inner lid. The inerting process is in accordance with the inerting process described in NUREG-1536 (Ref. D4.1.54, Sections 8.0 and V.1). After the waste package inner vessel is backfilled by helium, both the spread ring welds and the purge port plug are leak tested in accordance with *2001 ASME Boiler and Pressure Vessel Code* (Ref. D4.1.5, Section V, Article 10, Appendix IX) to verify that no leakage can be detected that exceeds the rate of  $10^{-6}$  std cm<sup>3</sup>/sec.

Waste package closure welding, nondestructive examination, stress mitigation, and inerting are conducted in accordance with approved administrative controls. The processes for waste package closure welding, nondestructive examination, stress mitigation, and inerting will be developed in accordance with the codes and standards identified below. The processes are monitored by qualified operators, and resulting process data are checked and verified as acceptable by qualified individuals.

Waste package closure welding, nondestructive examination, stress mitigation, and inerting normal operating procedures will specify, for example, the welding procedure specification, nondestructive examination procedure, qualification and proficiency requirements for operators and inspectors, and acceptance and independent verification records for critical process steps.

The waste package closure subsystem-related welds, weld repairs, and inspections are performed in accordance with *2001 ASME Boiler and Pressure Vessel Code* (Ref. D4.1.5, Section II, Part C; Section III, Division I, Subsection NC; Section IX; Section V).

The inerting of the waste package is performed in accordance with the applicable sections of NUREG-1536 (Ref. D4.1.54).

PCSA event sequences involving waste packages include challenges ranging from low velocity collisions to a 20 metric ton rockfall to a spectrum of fires. Waste package failure probabilities are calculated to be very low. Furthermore, a significant conservatism in the analysis is that the containment associated with the canister is not included in the probability of containment breach. In other words, if the waste package breaches, radionuclide release is analyzed as if the canister has breached (if the event sequence is in Category 1 or 2). Analytically, the canister is not relied upon for event sequences involving waste packages. The analytical results from the LLNL analysis show a significant reduction in canister strains is achieved by transportation cask and aging overpack protection. Although not analyzed, a similar ameliorating effect on the canister would be expected to be provided by the waste package.

The weld, inspection and repair process ensures no significant defects to a high reliability. The event sequence analysis shows that all event sequences associated with waste package breach are Beyond Category 2. In the context of the event sequence analysis, a significant defect is one that would have increased the probability of breach of the canister within the waste package by orders of magnitude. Even for significant weld defects, the protection offered by the waste package to the canister containment function would remain. Therefore, the effect of waste package weld failure on loss of canister containment during event sequences is not further considered.

#### **D1.4.6 Waste Package End-to-End Impact**

An oblique impact of a long naval SNF waste package inside TEV was modeled to assess the structural response (Ref. D4.1.19). Most of the model runs were made using an initial impact velocity of 3.859 m/sec, which corresponds to a drop height of 0.759 m (2.49 ft). The maximum ETF for the 3.859 m/sec (12.66 ft/sec) oblique impact in the OCB is about 0.7 (Ref. D4.1.19, page 37, Table 7-3, runs 1, 2, and 3), corresponding to a failure probability of approximately  $2 \times 10^{-5}$ . The oblique impact should be bounding for a direct end impact. Using equation D-4, an ETF of 0.11 is estimated for the hypothesized 3.4 mph end-to-end collision (two TEVs each traveling 1.7 mph), corresponding to a failure probability of less than  $1 \times 10^{-8}$ . The failure of the OCB is used to define the loss of containment, taking no credit for the inner vessel and the canister within. As was done for the results from LLNL, to introduce an additional measure of conservatism, a failure probability of  $1 \times 10^{-5}$  is used for the probability that the waste package containment would fail due to a 3.4 mph end-to-end impact.

### D1.5 PREDICTING OUTCOMES OF OTHER SITUATIONS BY EXTRAPOLATING STRAINS FOR MODELED SCENARIOS

Equation 17 in Section 6.3.2.2 demonstrates use of the probability of failure at a given drop height together with the COV to predict probabilities at other drop heights. A similar approach can be used to extrapolate from one strain to another to find the corresponding failure probability. The work done on damaging the container expressed in the form of strain should be roughly proportional to the energy input to the material due to the impact. The impact energy is proportional to the drop height or to the square of the impact velocity. Finite element modeling demonstrated that the increase in strain is actually less than proportional to increase in drop height (Ref. D4.1.27, Tables D1.2-3 and D1.2-4), so increasing the strain proportionally with drop height or the square of impact velocity is conservative. The strain is extrapolated by multiplying it by the square of the ratio of the velocity of interest to the reference velocity.

$$\tau_i = \tau_{ref} \left( \frac{v_i}{v_{ref}} \right)^2 \quad (\text{Eq. D-4})$$

where

- $\tau_i$  = strain at velocity of interest (dimensionless)
- $\tau_{ref}$  = strain at reference velocity (dimensionless)
- $v_i$  = velocity of interest (same units as  $v_{ref}$ )
- $v_{ref}$  = reference velocity (same units as  $v_i$ )

In case D.IC.3, a 0.16% strain ( $\tau_{ref}$ ) was predicted for a side impact of 40 ft/min ( $v_{ref}$ ). Using Equation D-4 to extrapolate for an impact velocity of 2.5 mph gives an estimated strain of 4.84%.

The estimated strain is then compared with the fragility curve tabulated in Figure D1.1-1. A failure rate of less than  $1 \times 10^{-8}$  is predicted for a strain of 4.84%. Probabilities of failure for a range of impact velocities are listed in Table D1.5-1.

Table D1.5-1. Calculated Strains and Failure Probabilities for Given Side Impact Velocities

Impact Velocity		% strain	Probability of failure
(ft/sec)	(ft/min)		
0.67	40	0.16	$< 1 \times 10^{-8}$
1	60	0.36	$< 1 \times 10^{-8}$
2	120	1.44	$< 1 \times 10^{-8}$
4	240	5.76	$< 1 \times 10^{-8}$
6	360	13	$< 1 \times 10^{-8}$
8	480	23	$< 1 \times 10^{-5}$

Source: Original

A similar approach is applied to estimate failure probabilities for vertical drops greater than 40 feet. The strains are extrapolated using the ratio of drop heights rather than the squared ratio of impact velocities in Equation D-4.

For the DPC, the maximum EPS is 2.65% for a 40-foot end drop (case D.IC.1b in Table D1.2-3). Strains of 2.98% and 3.31% are estimated for 45- and 50-foot drops, respectively. Doubling the strains to account for triaxiality and comparing these strains with Table D1.1-1 shows the probabilities of failure are both  $< 1 \times 10^{-8}$ . As before, conservative probabilities of  $1 \times 10^{-5}$  are used in the event sequence quantification.

For the DOE standard canister the maximum strain is 8% in the lower head of the 18-inch canister resulting from a 23-foot drop 3 degrees off vertical (Table D1.2-6). By the same approach as above, 10.4%, 15.7%, and 17.4% strains are estimated for 30-foot, 45-foot, and 50-foot drops. Doubling these strains and comparing with Table D1.1-1 yields the failure probabilities of  $1 \times 10^{-7}$ ,  $3 \times 10^{-2}$ , and  $9 \times 10^{-2}$  for the 30-foot, 45-foot, and 50-foot drops, respectively. A conservative probability of  $1 \times 10^{-5}$  is used for the 30-foot drop of the DOE standardized canister.

## **D1.6 MISCELLANEOUS SCENARIOS**

### **D1.6.1 Localized Side Impact on a Transportation Cask**

One of the requirements specified for transportation casks is they be robust enough to survive a 40-inch horizontal drop onto an unyielding 6-inch diameter upright cylinder (Ref. D4.2.2, Paragraph 71.73). The impact energy for such a scenario involving a 250,000 pound cask (a typical weight for a loaded cask) – the Nuclear Assurance Corporation STC has a loaded weight of 260,000 pounds (Ref. D4.1.50, p. 1.1-1) is about 1.1 MJ. The maximum weight of a forklift is considerably less than 20,000 kg. At a maximum speed of 2.5 mph (1.12 m/sec), the maximum impact energy would be 12.5 kJ, a factor of 90 less than the impact energy for the 40-inch drop of the cask. If the resultant strain is proportional to the impact energy and the drop event in the Safety Analysis Report (SAR) is just below the failure threshold (i.e., the median impact energy for failure), the impact energy due to the 2.5 mph impact would be a maximum of  $1/90^{\text{th}}$  of the median failure impact energy, or  $1 - 1/90$  COVs less than a normalized median of 1. Equation D-3 is applicable substituting the ratio of impact energy to median failure impact energy for the factor ETF. Using  $1/90$  ( $=0.011$ ) in place of the ETF in Equation D-3 gives a probability of failure of much less than  $1 \times 10^{-8}$  due to impact of a forklift against a transportation cask. If the impact speed were 9 mph instead of 2.5 mph, the impact energy would be about  $1/7^{\text{th}}$  of the energy in the SAR drop event, 0.14 would be used in place of the ETF in Equation D-3, and the probability of failure would still be less than  $1 \times 10^{-8}$ .

### **D1.6.2 Screening Argument for TAD Weld Defects**

TAD canister closure is the process that closes the loaded TAD canister by welding the shield plug and fully draining and drying the TAD canister interior, followed by backfilling the TAD canister with helium and fully welding the TAD canister lid around its circumference onto the body of the TAD canister.

The process control program for the closure welds produced by the TAD canister closure system is controlled as a special process by the Quality Assurance Program (Ref. D4.1.29, Section 9.0).

TAD canister closure is done at the TAD canister closure station in the Cask Preparation Area. The STC containing a loaded TAD canister is transferred from the pool to the TAD canister closure station using the cask handling crane. The STC lid is unbolted and then removed using the TAD canister closure jib crane. The TAD canister is then partially drained via the siphon port in order to lower the water level below the shield plug in preparation for welding. The TAD canister welding machine is positioned onto the TAD canister shield plug using the TAD canister closure jib crane, and the shield plug is welded in place. After a weld is completed, visual examination of the weld is performed in addition to the eddy current testing and ultrasonic testing that are performed by the TAD canister welding machine.

A draining, drying, and inerting system is connected to the siphon and vent ports in the shield plug and used to dry the interior of the TAD canister, followed by backfilling it with helium gas. Port covers are then placed over the siphon and vent ports and welded in place using the TAD canister welding machine. The TAD canister welding machine is removed, and the outer lid is placed onto the TAD canister using the TAD canister closure jib crane. The TAD canister welding machine is positioned onto the TAD canister outer lid, and the lid is welded in place. The TAD canister welding machine is removed, and the STC lid is placed onto the STC using the TAD canister closure jib crane and installed. Hoses are connected to the fill and drain ports on the STC, and the water is sampled for contamination. If the water is clean, the ports are opened to drain the annulus between the TAD canister and the STC. If the water is contaminated, then the annulus is flushed with treated borated water as needed. A drying system is then used to dry the annulus. The potential for contamination is kept to a minimum by the use of the inflatable seal.

The qualification of the TAD canister final closure welds is in accordance with ISG-18 (Ref. D4.1.55) as specified in *Basis of Design for the TAD Canister-Based Repository Design Concept* (Ref. D4.1.15, Section 33.2.2.36). Adherence to this guidance is deemed to provide reasonable assurance that weld defects occur at a low rate. However, TAD canister weld cracks are considered an initiating event after the TAD canister welding process in the Wet Handling Facility. If this occurs, the radionuclide release would be minimal because the incoming casks and canisters have already been opened. After TAD canisters are welded, they are placed in aging overpacks and moved by the site transporter to the CRCF. The probability of TAD canister failure during removal from the aging overpack handling in the CRCF and placement into a waste package is considered in the CRCF event sequence analysis. The conditional probability of TAD canister failures during handling in the CRCF has been shown to be small. The low probability of weld defects and their size would not alter this result. After the TAD canister is placed in the waste package, the containment is considered to be the waste package and the TAD canister is no longer relied upon in event sequences involving mechanical impacts.

## **D2 PASSIVE FAILURE DUE TO FIRE**

A risk assessment must consider a range of fires that can occur, as well as variations in the dynamics of the heat transfer and uncertainties in the failure temperature of the target. This section presents an analysis to determine the probability that a waste container will lose

containment integrity or lose shielding in a fire. Section D2.1 addresses loss of containment and Section D2.2 addresses loss of shielding.

## **D2.1 ANALYSIS OF CANISTER FAILURE DUE TO FIRE**

A common approach to safety analysis in regards to the effect of a fire is to postulate a specific fire (in terms of duration, combustible loading, heat rate, and other fire parameters) and then apply it to a specific configuration of a target. Then, a simple comparison is made between the temperature that the target reaches as a result of the fire, and the failure temperature of the target. Based on this comparison, a conclusion is made that either the target always fails, or never fails, or fails at some specific time. While such an approach may be appropriate for demonstrating that a specific design code has been met, it is not appropriate for a risk informed PCSA.

There are two parts to the assessment of the canister failure probability (sometimes referred to as the canister *fragility*): determining the thermal response of the canister to the fire and determining the temperature at which the canister will fail. In calculating the thermal response of the canister, variations in the intensity and duration of the fire are considered along with conditions that control the rate of heat transfer to the container (e.g., convective heat transfer coefficients, view factors, emissivities). In calculating the failure temperature of the canister, variations in the material properties of the canister material are considered along with variations in the loads that lead to failure.

### **D2.1.1 Uncertainty in Fire Severity**

In the fragility analysis, fire severity is characterized by the fire temperature and duration, since these factors control the amount of energy that the fire could transfer to a target cask or canister. Uncertainty distributions were developed for the fire temperature and fire duration based on a review of generic and YMP-specific information.

#### **D2.1.1.1 Uncertainty in Fire Duration**

In the context of this study, this duration of the fire is from the perspective of the target (i.e., the cask or canister that could be compromised by the fire). Therefore, the fire duration used in the analysis is the amount of time a particular container is exposed to the fire, and not necessarily the amount of time a fire burns. As an example, a fire that propagates through a building over a four-hour period is not a four-hour hazard to a particular target. In calculating the exposure time for a specific target, it does not matter whether the fire started in the room where the target is, or it started in another room and ended where the target is, or the fire passed through the target room between its beginning and end. The exposure duration is how long the fire burns while consuming combustibles in the vicinity of the target. This allows a single probability distribution to be developed for the fire duration, regardless of how the fire arrived at the target, based on estimates of the duration of typical single-room fires.

In order to develop this curve, data on typical fire durations is required. A number of sources were used to derive insights regarding the range of expected durations of typical fires. The following sources were used:

- NUREG/CR-4679 (Ref. D4.1.53) reviewed the results of fire tests conducted by a number of organizations on a variety of types and amounts of combustible materials. Although focused on nuclear power plants, the materials assessed are typical of those found at a variety of industrial facilities.
- NUREG/CR-4680 (Ref. D4.1.52) reports on the results of a series of tests conducted by Sandia National Laboratories using a series of fuel source packages representative of trash found around nuclear power plants. Once again, these packages are typical of what might be found around other types of industrial facilities.

The tests were not extensive, and represented only particular configurations. In general, the fire durations were found to depend upon the amount, type, and configuration of the available combustible material.

Based on a review of the available information, it was determined that two separate uncertainty distributions (i.e., probability distributions that represent uncertainty) would be needed: one for conditions without automatic suppression and one for conditions with automatic suppression. The derivation of these two distributions is discussed below.

#### **D2.1.1.2 Fire Duration without Automatic Fire Suppression**

The first uncertainty distribution was developed for fires in which automatic fire suppression is not available. The vast majority of the tests conducted were for this case. The following summarizes information presented in the three references listed above.

Sandia National Laboratories conducted two large-scale cable fire tests using an initial fire source of five gallons of heptane fuel, and an additional fuel loading of two vertical cable trays with a 12.5% fill consisting of 43 10-foot lengths of cable per tray (Ref. D4.1.53, Section 2.2.1). The only difference between the tests was that one test used unqualified cable and the other used IEEE-383 qualified cable. In the unqualified cable test, the cables reached peak heat release at approximately four minutes, and the rate decayed toward reaching zero at approximately 17 minutes. In the qualified cable test, the cables reached peak heat release at approximately seven minutes, and the rate decayed toward reaching zero at approximately 16 minutes.

Factory Mutual Research Corporation conducted tests for large-scale configurations of cable trays (Ref. D4.1.53, Section 2.2.3). One set of tests involved a configuration of 12 fully loaded horizontal trays in two stacked tiers. NUREG/CR-4679 (Ref. D4.1.53) provides detailed results for three of the “free-burn” tests (no automatic fire suppression). The first test reached and maintained the peak heat release rate at six minutes to 20 minutes, and reached zero at 25 minutes. The second test reached and maintained the peak heat release rate at seven minutes to 25 minutes, and reached zero at 34 minutes. The third test reached and maintained the peak heat release rate at 26 minutes to 40 minutes, and reached zero at 60 minutes.

Lawrence Berkeley Laboratory conducted tests on electrical cabinets (Ref. D4.1.53, Section 2.2.5). Two tests were conducted. The first was a single cabinet with only thermocouple wire and leads and no internal cabinet fuel loading. The fire that exposed the cabinet was two trash bags with loosely packed paper in a 32-gallon polyethylene trash receptacle, plus two cardboard boxes of packing “peanuts.” This fire reached a peak heat release rate at seven minutes, and reached zero at 19 minutes. The second test involved two cabinets separated by a steel barrier. The cabinets contained a total of 64 lengths of cable (48 and 16). The source fire in this test was similar in nature to the first test, but had a heavier container and loose paper instead of the “peanuts.” This fire had two peaks, at six minutes and 18 minutes, with the second being much larger than the first. The fire decayed toward reaching zero between 25 minutes and 30 minutes.

The Department of Health and Human Services sponsored a series of tests on various types of furnishing materials (Ref. D4.1.53, Section 3). While the specific types of furnishings are unlikely to be found in a YMP preclosure facility, these results are instructive for combinations of combustible materials that could be found. The first test was on a molded fiberglass chair with a metal frame. The fire reached a peak heat release rate in two minutes, and reached zero at 10 minutes. The second test was for a wood frame chair with latex foam cushions. This fire reached a peak heat release rate in four minutes and reached zero at 40 minutes. The final test was on four stackable, metal frame chairs with cushions that appeared to consist of a wood base, foam core, and vinyl cover. The fire reached a relatively steady state peak heat release rate from four minutes to 23 minutes, and reached zero at 38 minutes.

Sandia National Laboratories performed a series of nine tests on representative transient fuel fires (Ref. D4.1.52). Five different fuel packages were used for the tests. The first two fuel packages used mixed wastes representative of cleaning materials that might be left by maintenance personnel during routine operations. The first package was about 1.8 kg, and the second about 2.2 kg. The other difference between the two packages was the first package had more cardboard, whereas the second had more plastic. In both tests on the first package, the fire reached a peak heat release rate at approximately four minutes. However, they reached zero at different times (greater than 30 minutes versus approximately 20 minutes). In the two tests on the second package, the time of peak heat release was different (a high peak at four minutes versus a relatively low peak at 10 to 20 minutes), but they both reached zero at approximately the same time (50 minutes).

The third fuel package was designed to represent normal combustibles that might be in control or computer rooms, and consisted primarily of cardboard and stacked paper, with some crumpled paper. Total mass was about 7.9 kg. In both tests, the fire reached a peak heat release rate in approximately two minutes, but reached zero at different times (16 minutes versus 20 minutes).

The fourth fuel package was designed to represent mixed waste that might be found in a control room, computer room, security room, or similar location. It consisted primarily of a plastic trash can filled with paper and rags. Total mass was about 1.6 kg. In both tests, the fire reached a peak heat release rate in approximately three minutes and remained relatively steady for most of the duration of the fire, but reached zero at different times (54 minutes versus 70 minutes).

The fifth fuel package was designed to represent larger industrial waste containers that might be found in a variety of places in an industrial facility. It consisted primarily of a large plastic receptacle filled with wood, cardboard, paper, and oily rags. Total mass was about 6.5 kg. Only one test was conducted with this fuel package, and the fire reached two separate peak heat release rates (at 35 and 50 minutes) and decayed toward reaching zero at 80 minutes.

The preceding test data were reviewed and a probability distribution for the fire duration was developed based on engineering judgment. This distribution is characterized by 10% to 90% hazard levels of 10 minutes and 60 minutes, respectively (i.e., it was concluded that 10% of the fires would result in a target exposure duration of less than 10 minutes and 90% of the fires would result in a target exposure duration of less than 60 minutes). These values were fitted to a lognormal distribution with a mean and standard deviation of 3.192 and 0.6943, respectively. The mean of this distribution is approximately 31 min, the median (50<sup>th</sup> percentile) is approximately 24 min, and the error factor (i.e., the ratio of the 95<sup>th</sup> percentile over the median) is about 3.1. The resultant probability distribution is presented in Table D2.1-1 as the probability of target exposure durations over a set of discrete intervals. The 30-minute design basis fire duration mandated in 10 CFR 71.73 (Ref. D4.2.2) corresponds to the 62<sup>nd</sup> percentile value of this distribution.

Table D2.1-1. Probability Distribution for Fire Duration - Without Automatic Fire Suppression

Fire Duration (min)	Cumulative Probability	Fire Duration Interval (minutes)	Interval Probability <sup>a</sup>
10	0.1	0 to 10	0.1
20	0.39	10 to 20	0.29
30	0.62	20 to 30	0.23
40	0.76	30 to 40	0.14
50	0.85	40 to 50	0.09
60	0.903	50 to 60	0.053
70	0.936	60 to 70	0.033
90	0.97	70 to 90	0.034
120	0.989	90 to 120	0.019
150	0.9956	120 to 150	0.0066
180	0.998	150 to 180	0.0024
210	0.999	180 to 210	0.001
270	0.99974	210 to 270	0.00074
360	0.99995	270 to 360	0.00021
∞	1	>360	5E-05

NOTE: <sup>a</sup>The interval probability is the difference between the cumulative probability at the top of the interval and the cumulative probability at the bottom of the interval.

Source: Original

### D2.1.1.3 Fire Duration with Automatic Suppression

The second uncertainty distribution that was developed is for fires where automatic suppression is available. There were only a limited number of tests conducted for this case.

Factory Mutual Research Corporation conducted tests for large-scale configurations of cable trays, as discussed in the previous sections. In addition to the tests conducted without suppression, a number of tests were conducted with suppression. NUREG/CR-4679 (Ref. D4.1.53, pp. 26-31) provides detailed results for six of these “extinguishment tests.” All these tests involved a configuration of 12 fully loaded horizontal trays in two stacked tiers. Two of the six also involved the addition of two fully loaded vertical cable trays. The cables were polyvinyl chloride (PVC) - jacket with polyethylene insulation. The results of the first four tests were that the fires reached their peak heat release rates at 8, 9, 12, and 12 minutes. The associated times when the heat release rate dropped to zero were 10, 12, 16, and 29 minutes, respectively. The results of the final two tests were peak heat release rates at 9 and 16 minutes, with zero being reached at 24 and 36 minutes, respectively.

These were the only extinguishment tests reported in the references. Therefore, an analysis of a wooden box-type fire conducted by Parsons also was examined. This is not an actual test, but rather a calculation of a “typical” fire where credit was given for the actuation of fire suppression. The calculation gave a peak heat release rate occurring at seven minutes and extending to 15 minutes. The calculation showed the fire decaying towards zero at approximately 20 minutes.

These test data were reviewed and a probability distribution for the fire duration was developed based on engineering judgment. Although the data are somewhat sparse, they were taken in the overall context of how the actuation of suppression affected the tests conducted and how that compared to the free-burn tests. This was extrapolated to the other free-burn tests. It was judged likely that the operation of automatic suppression would have little effect on the lower end of the distribution, as such fires would likely burn out without actuating suppression. However, there would be a significant effect for the longer fires. It was concluded that a reasonable estimate of the 10 to 90% hazard levels was 10 minutes and 30 minutes (i.e., it was concluded that it was a reasonable interpretation of the data to state that 10% of the fires would result in target exposure duration of less than 10 minutes and 90% of the fires would result in target exposure duration of less than 30 minutes). These values were fitted to a lognormal distribution with a mean and standard deviation of 2.849 and 0.4286, respectively. The resultant uncertainty distribution is presented in Table D2.1-2 as the probability of target exposure durations over a set of discrete intervals.

Table D2.1-2. Probability Distribution for Fire Duration - With Automatic Fire Suppression

Fire Duration (min)	Cumulative Probability	Fire Duration Interval (min)	Interval Probability <sup>a</sup>
10	0.1	0 to 10	0.1
15	0.37	10 to 15	0.27
20	0.63	15 to 20	0.26
25	0.81	20 to 25	0.18
30	0.901	25 to 30	0.091
40	0.975	30 to 40	0.074
50	0.993	40 to 50	0.018
60	0.9982	50 to 60	0.0052

Table D2.1-2. Probability Distribution for Fire Duration - With Automatic Fire Suppression (Continued)

Fire Duration (min)	Cumulative Probability	Fire Duration Interval (min)	Interval Probability <sup>a</sup>
80	0.9998	60 to 80	0.0016
100	0.99998	80 to 100	0.00018
∞	1	>100	2E-05

NOTE: <sup>a</sup>The interval probability is the difference between the cumulative probability at the top of the interval and the cumulative probability at the bottom of the interval.

Source: Original

### D2.1.2 Uncertainty in Fire Temperature

As used in the fire fragility analysis, the fire temperature is the effective blackbody temperature of the fire. This temperature implicitly accounts for the effective emissivity of the fire, which for large fires approaches a value of 1.0 (Ref. D4.1.61, p. 2-56). A review of the available fire temperature data for liquid and solid fuels is discussed below.

Experimental measurements of liquid hydrocarbon pool fires with radii from 0.25 to 40.0 m indicate effective blackbody radiation temperatures between 1,200 K and 1,600 K (927°C and 1,327°C) (Ref. D4.1.61, p. 2-56). Testing of rail tank cars engulfed in a liquid hydrocarbon pool fire indicates an effective blackbody temperature of 816°C to 927°C (1,089 K to 1,200 K) (Ref. D4.1.2).

Heat release data for combustible solid materials such as wood, paper, or plastic are plentiful, but fire temperature data have generally not been presented. However, *The SFPE Handbook of Fire Protection Engineering* (Ref. D4.1.61, pp. 3-82 to 3-87) discusses the hot gas temperatures associated with fully-developed compartment fires that do include combustion of solid materials. Fully-developed fires involve essentially all combustible material in a compartment, so the peak hot gas temperature should be reasonably indicative of the *effective* fire temperature. The data indicate typical peak temperatures between 400°C and 1,200°C (750°F and 2,190°F). (The 400°C value applies to small, short duration fires and is too low to represent a true fire temperature.)

Fires within one of the YMP facilities are likely to involve both combustible solid and liquid materials. Judgment suggests that most postulated fires should generally resemble the compartment fires discussed in *The SFPE Handbook of Fire Protection Engineering* (Ref. D4.1.61, Section 2, Chapter 7). This implies that the assigned temperature distribution should be strongly influenced by the 400°C and 1,200°C range. However, combustible liquids (e.g., diesel fuel in a site transporter) may also contribute significantly to some fires, so the upper bound of the fire temperature distribution should include the higher temperatures indicated by the pool fire data. Based on this reasoning, the fire temperature distribution is normally distributed with a mean of 1,072 K (799°C) and a standard deviation of 172 K. The mean of this distribution is approximately equal to the transportation cask design basis fire temperature of 800°C mandated in 10 CFR 71.73 (Ref. D4.2.2).

This fire temperature probability distribution has a value of 400°C for the 5th percentile and 1,327°C for the 99.9th percentile. The first value represents the lower end of the compartment fire temperature range while the second corresponds to the upper end of the liquid pool fire effective blackbody temperature range. Therefore, the distribution applies to fires involving both liquid and solid fuels.

It should be noted that data from fire testing indicate that the fire temperature is not constant over the duration of the fire. The fire temperature generally increases to a peak value and then decreases considerably as the combustible material is consumed. In the fire fragility analysis, herein, the fire temperature is treated as constant, which tends to increase the maximum target temperature.

### **D2.1.3 Correlation of Fire Temperature and Duration**

Testing has shown that fire temperature and duration are negatively correlated. Intense fires with high fire temperatures tend to be short-lived because the high temperature results from very rapid burning of the combustible material. In contrast, long duration fires generally result from slower burning of the combustible material. In the probabilistic fire fragility analysis discussed below, the fire temperature and duration were correlated with a conservative correlation coefficient of -0.5. It is conservative because this correlation allows some fires that have both a high temperature and long duration.

### **D2.1.4 Uncertainty in the Thermal Response of the Canister**

The probability distributions discussed in Section D2.1.1 characterize the uncertainty in the fire severity. In order to determine the probability that a canister fails due to a fire, models are needed to calculate the uncertainty in the thermal response of the container to a fire and the uncertainty in the failure temperature of the container.

The following sections describe the two simplified heat transfer models used to determine the thermal response of the canister to the fire. The heat transfer models have been simplified in order to allow a probabilistic analysis using Monte Carlo sampling. The two models discussed below apply to bare canisters or canisters inside a waste package, transportation cask, or a canister transfer machine (CTM) shielded bell. The simplified model was validated by comparison with a more complete model as discussed in Section D2.1.4.3.

#### **D2.1.4.1 Heat Transfer to Bare Canisters**

Bare canisters near or engulfed in a fire can be heated primarily by two heat transfer mechanisms: convection and radiation. Convection heating occurs when hot gases from the fire circulate and come into contact with the canister surface. Due to gravitational effects, the hot gases from the fire are expected to rise and collect near the ceiling of the room. Thus, unless a canister is engulfed in the fire, the hot gases are unlikely to come into direct contact with the canister, and radiation should be the dominant mode of heating. Further, radiation from the flame (luminous portion of the fire gases) is expected to far exceed radiation from the hot gas layer near the ceiling. For that reason, radiative heating by the hot gas layer is not considered in

the fragility analysis. The heat transfer model described in the following sections is believed to capture the important aspects of the heat transfer from the fire.

Due to substantial conduction within the metal wall of the canister, the canister wall is modeled as a single effective temperature (thin-wall approximation) during heatup. Using this approach, the canister temperature ( $T_c$ ) was advanced in time using the following Euler finite-difference formulation:

$$T_c = \frac{q_{c,net} \Delta t}{m_c c_{p,c}} + T_{c,i} \quad (\text{Eq. D-5})$$

where

- $m_c$  = mass of the canister wall
- $c_{p,c}$  = specific heat of the canister material
- $\Delta t$  = time step
- $T_{c,i}$  = canister temperature at the beginning of the time step, and
- $q_{c,net}$  = net rate of energy deposition into the canister.

The net rate of energy deposition into the canister during the fire is given by the following equation:

$$q_{c,net} = q_{r,fire} + q_{c,fire} - q_{r,f} \quad (\text{Eq. D-6})$$

where

- $q_{r,fire}$  = radiative heat transfer to the canister from the fire
- $q_{c,fire}$  = net convective heat transfer to the canister (positive if the canister is engulfed by the fire and negative if the canister is not engulfed by the fire)
- $q_{r,f}$  = radiative heat transfer from the canister to material stored in the canister.

The terms on the right-hand-side of this equation are defined below.

An earlier formulation of Equation D-6 included convective heat transfer from the canister wall to the gas inside the canister and from this gas to the spent fuel inside the canister. The addition of this heat transfer term did not significantly affect the heating rate of either the canister or the fuel, but did significantly increase the calculation time for the analysis. For that reason, convective heat transfer to the gas inside the canister was not included in the subsequent probabilistic analysis.

In this analysis, the important parameters are: (1) the fire temperature, size, and location relative to the canister, (2) treatment of the fire surface as a blackbody, and (3) treatment of the canister surface as diffuse and gray. Thus, the net rate of radiative heat transfer to the canister surface,  $q_{r,fire}$ , is given by:

$$q_{r,fire} = \epsilon_c A_c F_{c-fire} F_s \sigma (T_{fire}^4 - T_c^4) \quad (\text{Eq. D-7})$$

where

$\epsilon_c$	=	emissivity of the canister surface
$A_c$	=	surface area of the canister
$F_{c-fire}$	=	view factor between the canister and the fire, which is the related to the fraction of radiation leaving the fire that strikes the canister surface
$F_s$	=	suppression scale factor (discussed below)
$\sigma$	=	Stefan-Boltzmann constant
$T_{fire}$	=	effective blackbody temperature of the fire
$T_c$	=	canister temperature.

In Equation D-6,  $q_{c,fire}$  is the energy input due to convective heating from the fire, which is given by:

$$q_{c,fire} = A_c F_s h_{conv} (T_{fire} - T_c) \quad (\text{Eq. D-8})$$

where  $h_{conv}$  is the convective heat transfer coefficient and all other terms are defined as above.

The final term in Equation D-6 is the rate of heat transfer from the canister to the spent fuel or HLW. This term is given by the following equation:

$$q_{r,f} = \frac{A_c F_{c-f} \sigma (T_c^4 - T_f^4)}{1/\epsilon_c + 1/\epsilon_f - 1} \quad (\text{Eq. D-9})$$

where  $F_{c-f}$  is the view factor between the canister and the fuel,  $\epsilon_f$  is the emissivity of the fuel, and  $T_f$  is the temperature of the fuel being heated by the canister (outer portion of the fuel).

As the canister becomes hotter and heat is transferred to the fuel, the fuel temperature will also increase according to the following equation:

$$T_f = \frac{(q_{r,f} + q_{DH})\Delta t}{m_f c_{p,f}} + T_{f,i} \quad (\text{Eq. D-10})$$

where  $q_{DH}$  is the decay heat generated in the fuel,  $m_f$  is the mass of fuel heated by the canister (outer portion of the fuel),  $c_{p,f}$  is the specific heat of the fuel, and  $T_{f,i}$  is the fuel temperature at the beginning of the time step.

Equation D-10 uses the mass of fuel being heated by the canister and the corresponding decay heat in this portion of the fuel. This equation ignores heat transfer from the heated fuel to unheated fuel. That is, there is no energy exchange between the outer fuel and the inner fuel.

The fuel mass to use in Equation D-10 can be estimated by calculating the thermal penetration depth within the fuel during the fire. In a number of previous studies (for example, (Ref. D4.1.25)), the fuel region inside the canister has been treated as a homogeneous material with effective thermal properties. The effective thermal properties used in these studies were determined for many different fuel configurations based on the results from detailed thermal analyses. Table D2.1-3 presents the effective thermal properties for 21-PWR fuel in the TAD canister (Ref. D4.1.25).

Table D2.1-3. Effective Thermal Properties for 21-PWR Fuel in a TAD Canister

Property	Value
Density, $\rho$	3,655 kg/m <sup>3</sup>
Specific Heat, $c_p$	438 J/kg K
Thermal Conductivity, $k$	4.29 W/m K
Thermal Diffusivity, $\alpha$	$2.6 \times 10^{-6}$ m <sup>2</sup> /sec

NOTE: PWR = pressurized water reactor; TAD = transportation, aging, and disposal (canister)

Source: Ref. D4.1.25, Table 17, and Equation 2 of Section 6.2.2

Based on the effective thermal properties listed in the table, estimation of the thermal penetration depth during a typical fire is given by the following equation:

$$\delta = \sqrt{\alpha t} \quad (\text{Eq. D-11})$$

where  $\alpha$  is the effective thermal diffusivity and  $t$  is the time (3,600 seconds). Based on the effective thermal diffusivity shown in the table, a thermal penetration depth of approximately 9.5 cm is calculated. The fuel volume corresponding to this penetration depth is calculated by multiplying the canister interior surface area by the penetration depth. The effective fuel mass is then calculated by multiplying this volume by the effective density of the fuel. The resulting fuel mass is approximately 9,700 kg.

#### D2.1.4.2 Heat Transfer to a Canister inside a Cask, Waste Package, or Shielded Bell

The calculation of the heating of a canister inside another container or structure is slightly more complex than that for a canister directly exposed to fire. When inside another container, the canister is not directly heated by the fire. Rather, the container is first heated by the fire and then the interior surface of the heated container radiates heat to the canister and also convects heat to any air or other gas in the annular region between the outer container and canister. When there are multiple heat transfer barriers (e.g., the waste package, which has an outer barrier and an inner barrier), heat transfer between the barriers must also be considered. The following discussion includes the presence of an inner and outer barrier, as is the case for a waste package.

The calculation of canister heating was accomplished by first calculating the temperature of the outer barrier when exposed to a fire. Then, the energy radiated from the outer barrier to the inner barriers was calculated. Next, the energy radiated from the inner barrier to the canister was calculated. Models that included convective heat transfer to and from the gas in the annular spaces between these regions demonstrated that convective heating and cooling had little effect

on the heating of the canister, but caused calculation times to be significantly longer. As a result, the convective heat transfer was removed from the models and the temperature increase of the inner barrier and canister were calculated based on radiative heating only.

It should also be noted that many transportation casks have neutron or gamma shielding composed of a low melting point material such as borated polyethylene. This material is likely to melt very quickly so its effect on heat transfer was not considered in the model. In reality, this layer of material would have a substantial resistance to heat transfer, at least initially. Ignoring this thermal resistance is therefore conservative.

The heating of the outer barrier is calculated in the same general manner as that of a bare canister exposed directly to a fire. Due to the substantial conduction within the metal barrier, the thin-wall approximation was applied. Using this approach, the outer barrier temperature ( $T_{ob}$ ) was advanced in time using the following Euler finite-difference formulation:

$$T_{ob} = \frac{(q_{ob} - q_{ib})\Delta t}{m_{ob} c_{p,ob}} + T_{ob,i} \quad (\text{Eq. D-12})$$

where

- $q_{ob}$  = radiation and convection to the outer barrier from the fire
- $q_{ib}$  = radiation to the inner barrier from the outer barrier
- $m_{ob}$  = mass of the outer barrier
- $c_{p,ob}$  = specific heat of the outer barrier
- $\Delta t$  = time step
- $T_{ob,i}$  = outer barrier temperature at the beginning of the time step.

Equation D-12 does not consider convective heat transfer to the air inside the container. Initial calculations showed that convective heat transfer to the air in the container would be small compared to the radiation heat loss term, so convective heat transfer was neglected.

If (1) the fire temperature, size, and location relative to a container are known, (2) the fire surface can be treated as a blackbody, and (3) the outer barrier surface can be considered diffuse and gray, then the net rate of radiative heat transfer to the outer barrier surface ( $q_{ob}$ ) can be approximated as:

$$q_{ob} = \varepsilon_{ob} A_{ob} F_{fc} F_s \sigma (T_f^4 - T_{ob}^4) \quad (\text{Eq. D-13})$$

where

- $\varepsilon_{ob}$  = emissivity of the outer barrier surface
- $A_{ob}$  = surface area of the outer barrier
- $F_{fc}$  = view factor for radiative heat transfer, which is related to the fraction of radiation leaving the fire that strikes the outer barrier surface

$F_s$	=	suppression scale factor (discussed below)
$\sigma$	=	Stefan-Boltzmann constant
$T_f$	=	fire (flame) temperature
$T_{ob}$	=	temperature of the outer barrier.

Once the temperature of the outer barrier is known, the heating of the inner barrier can be found in the same manner. Instead of a fire temperature, the temperature of the heated outer barrier is used and the net rate of radiative heat transfer from the outer barrier interior surface to inner barrier ( $q_{ib}$ ) can be approximated as:

$$q_{ib} = \frac{A_{ob} F_{oi} \sigma (T_{ob}^4 - T_{ib}^4)}{1/\epsilon_{ib} + 1/\epsilon_{ob} - 1} \quad (\text{Eq. D-14})$$

where

$\epsilon_{ib}$	=	emissivity for of the inner barrier
$F_{oi}$	=	view factor for radiation between the outer and inner barriers (discussed below)
$T_{ib}$	=	inner barrier surface temperature.

The temperature of the inner barrier is calculated using an equation similar to Equation D-12; however, in this equation, the thermal radiation incident on the inner barrier comes from the outer barrier rather than the fire and the heat loss from the inner barrier is to the spent fuel or HLW canister.

Finally, the temperature of the canister is calculated using the following equation, which has a form similar to Equation D-12:

$$T_c = \frac{(q_{ib} + q_{DH})\Delta t}{m_c c_{p,c}} + T_{c,i} \quad (\text{Eq. D-15})$$

where  $q_{DH}$  is the total decay heat generated by the contents of the canister and all other terms are defined as in preceding equations.

In Equation D-15, the heat capacity of the contents of the canister is conservatively neglected so that all decay heat is transmitted to the canister wall. In reality, some fraction of the decay heat would be transmitted to the contents of the canister (e.g., the spent fuel or HLW), increasing the temperature of the contents. Neglecting this term is conservative since it increases the temperature increase of the canister itself.

Note also that, in order to simplify the model, heat transfer from the canister to its contents is ignored in Equation D-15. In reality, some heat would be transferred from the canister wall to the spent fuel or HLW inside the canister. Neglecting this heat removal is conservative since it increases the temperature increase of the canister.

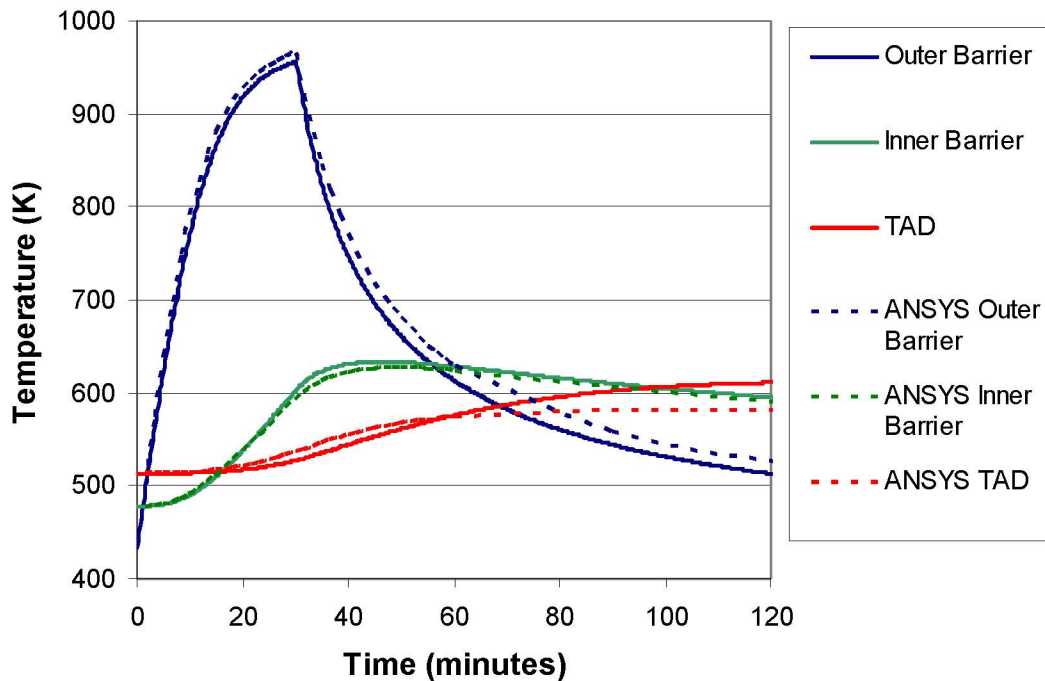
Unlike the bare canister case in which heating of the canister ends when the fire ends, heating of a canister that is inside other containers will increase after the fire ends as heat is transmitted from the heated outer and inner barrier. After the fire has been extinguished, heat will be lost by the outer barrier due to a combination of radiation to cooler surfaces and convection to the air in the room. A temperature of 400 K was used as the surface and air boundary condition. The surfaces were modeled as blackbodies in the radiation heat transfer calculation. Convective heat transfer was calculated based on a heat transfer coefficient of  $2.0 \text{ W/m}^2 \text{ K}$ . The fragility analysis showed that the predicted canister failure probability was not sensitive to either the boundary condition temperature or the convective heat transfer coefficient.

#### **D2.1.4.3 Validation of the Simplified Heat Transfer Models**

In order to validate the simplified heat transfer models discussed above, results were compared to results calculated using more detailed models. In one such comparison, results calculated using the model for heating of a canister in a waste package were compared to the results from a similar ANSYS calculation (Ref. D4.1.25, Attachment V). ANSYS is a finite-element analysis software application use in nuclear facility and non-nuclear industrial applications to model temperature evolutions of complex systems. The simplified model was set up to match the inputs to the ANSYS calculation as closely as possible. The only differences between the two included:

- The ANSYS run was made with temperature-dependent specific heats whereas average specific heats were used in the simplified model.
- The ANSYS run treated the TAD canister and its contents as a homogeneous material with average properties, whereas the simplified model treated the TAD canister but ignored heat transfer to its contents.

Figure D2.1-1 shows a comparison of the calculated time-dependent temperatures from these two calculations. The figure shows that the simplified model accurately predicts the results from the more detailed analysis. Because heat transfer from the TAD canister to its contents is ignored in the simplified model, the canister reaches slightly higher temperatures with the simplified model compared to the more detailed model.



NOTE: TAD = transportation, aging, and disposal (canister).

Source: Original

Figure D2.1-1. Comparison Between Results Calculated Using the Simplified Heat Transfer Model and ANSYS – Fire Engulfing a TAD Canister in a Waste Package

A similar comparison was made between the results reported in the HI-STAR SAR (Ref. D4.1.38, Table 3.5.4) and results calculated using the simplified model. These calculations simulated a design basis 30-minute fire. The maximum canister temperature reported in the HI-STAR SAR was 419°F (215°C). This temperature was predicted to occur approximately 3 hours after the start of the fire. The simplified model predicted a peak canister temperature of 213.5°C at approximately 4 hours after the start of the fire. This comparison again demonstrates the accuracy of the simplified model in predicting the maximum canister temperature due to the fire.

Detailed ANSYS calculations were not performed for the bare canister configuration. However, it is possible to infer the accuracy of the simplified bare canister model based on the accuracy of the simplified model in predicting the thermal response of the outer barrier in the waste package configuration. As shown in Figure D2.1-1, the simplified heat transfer accurately predicted the thermal response of the outer barrier both during the 30-minute fire and after.

#### D2.1.4.4 Heat Transfer Model Inputs and Uncertainties

The heat transfer models discussed in Sections D2.1.4.1 and D2.1.4.2 include a large number of input parameters. Some of these parameters are known to a high degree of confidence whereas

others are considered to be uncertain. This uncertainty was explicitly considered in the probabilistic analysis discussed in Section D2.1.1. The following sections discuss the major inputs to the models and the treatment of the uncertainty in these inputs.

#### **D2.1.4.4.1 View Factor**

The radiation view factor from the container (e.g., cask or waste package) to the fire can be calculated if the size of the fire and distance between the fire and the container can be determined. The size (height and width) of the fire can be approximated using published correlations in the SFPE handbook (Ref. D4.1.61, Section 1, Chapter 6). The distance between the fire and the container depends on the location of combustible materials and ignition sources relative to the container.

Since the location of combustible materials and ignition sources relative to the container is difficult to predict and would vary from one room to another, a conservative approach in which the container was engulfed by the fire is followed. For a container completely engulfed by the fire the view factor is essentially 1.0. This is conservative for the long vertically-oriented containers because even an engulfing fire may engulf only the lower portion of the container.

A view factor of 1.0 was applied only to the cask, waste package, or a shielded bell that encase a canister. Bare canisters are treated differently. Since a canister is only bare as it is being withdrawn from a cask or inserted into a waste package, only a portion of the canister could be exposed to the fire at any given time. In this case, the view factor is given by fraction of the canister actually exposed to the fire. This fraction depends on the space between the top of the cask or waste package and the ceiling of the loading or unloading room. Generally, this fraction would be considerably less than 50%.

The radiation view factor between concentric cylinders (e.g., the inner and outer barrier of a waste package) can be estimated very easily if the cylinders are very long compared to their diameters. Under this condition, which is true of most configurations of interest in the current study, the view factor can be approximated by  $D_i/D_o$ , where  $D_i$  and  $D_o$  are the inner and outer diameters of the two cylinders (Ref. D4.1.63, Configuration C-63).

#### **D2.1.4.4.2 Consideration of Fire Suppression on Canister Heating**

The effect of fire suppression on canister heating is treated using a suppression scale factor. The suppression scale factor is included in the heat transfer equations as an adjustment to the rate of heat transfer to the canister from the fire. The value of the suppression scale factor used in the model is based on testing at the Building and Fire Research Laboratory, which is part of the National Institute of Standards and Technology (Ref. D4.1.31).

The Building and Fire Research Laboratory tests considered a range of fires and a range of sprinkler system spray densities. Results were presented for the net heat release rate from the fire both before and after actuation of the fire suppression system. The fire suppression scale factor implicitly includes consideration of the time delay before actuation of the fire suppression system and the effectiveness of the system. Rooms with early actuation and effective fire suppression would have a very small suppression scale factor, whereas rooms with delayed

actuation and/or ineffective fire suppression would have a large suppression scale factor (upper bound of 1.0 when no suppression is present).

Because no credit is taken for fire suppression in this analysis, the fire suppression scale factor was set equal to 1.0 in all of the analyses discussed in this document.

#### **D2.1.4.4.3 Convective Heat Transfer Coefficient during the Fire**

In testing of containers engulfed in a fire, considerable variations in the convective heat transfer coefficient have been measured. Values as high as  $30 \text{ W/m}^2 \text{ K}$  have been measured in vigorously burning pool fires (Ref. D4.1.51, pp. 19-21), although values on the order of  $20 \text{ W/m}^2 \text{ K}$  or less are considered more typical (Ref. D4.1.57, Table 3-2). For fire conditions in which the combustible material is burning more slowly, values on the order of  $5 \text{ W/m}^2 \text{ K}$  or lower have been measured (Ref. D4.1.51, p. 19). To capture the potential variability in the convective heat transfer coefficient, a probability distribution for the convective heat transfer coefficient was included in the model. A normal distribution applies with a mean and standard deviation of  $17.5 \text{ W/m}^2 \text{ K}$  and  $4.2 \text{ W/m}^2 \text{ K}$ , respectively. This distribution yields practical upper and lower bound values (0.1 and 99.9th percentiles) of approximately 5 and  $30 \text{ W/m}^2 \text{ K}$ .

#### **D2.1.4.4.4 Decay Heat**

The canisters processed through the preclosure facilities will contain spent fuel with varying decay heat levels. Based on information provided in the safety analysis reports for transportation casks, a probability distribution was developed for the decay heat level in the canister. A normal distribution applies with a mean and standard deviation of 17 kW and 3 kW, respectively. This distribution yields practical upper and lower bound values (0.1 and 99.9th percentiles) of approximately 8 kW and 26 kW.

#### **D2.1.4.4.5 Other Model Inputs**

Other inputs required by the heat transfer model include (1) the thermal and physical properties of all materials, (2) the dimensions of the canister, cask, waste package, or shielded bell, (3) the initial temperatures of each layer, (4) decay heat generated within the canister, and (5) the post-fire convective heat transfer coefficient and temperature. The values for these input parameters are provided in Tables D2.1-4 through D2.1-7. The tables also provide a brief rationale or a reference for the values used in the analysis.

As shown in the tables, calculations were performed for two spent fuel canister (SFC) wall thicknesses: 0.5 inches (0.0127 m) and 1.0 inch (0.0254 m). This was done for two reasons. First, initial calculations showed that the wall thickness greatly influences both the heating and failure of the canister. Second, a review of the available canister information indicated a range of canister thicknesses from 0.5 inches to 1 inch. A substantial fraction of the older transport cask designs have SFCs with wall thicknesses of 0.5 or 0.625 inches, whereas newer designs (e.g., the naval SFC or TAD canister) are expected to have a wall thickness of 1.0 inch.

Table D2.1-4. Model Inputs – Bare Canister

Model Parameter	Value	Basis/Rationale
<b>Canister Properties</b>		
Outer diameter (m)	1.68	Minimum outer diameter listed in <i>Transportation, Aging and Disposal Canister System Performance Specification</i> (Ref. D4.1.28, Section 3.1.1)
Wall thickness (m)	0.0127 or 0.0254	0.5 inches is the thinnest canister wall thickness listed for current transport cask designs 1.0 inch is the anticipated TAD canister thickness and is also the thickness of the naval SFC
Length (m)	5.4	Typical length of TAD canister listed in <i>Transportation, Aging and Disposal Canister System Performance Specification</i> (Ref. D4.1.28, Section 3.1.1)
Density (kg/m <sup>3</sup> )	7980	Density of Type 316 stainless steel (Ref. D4.1.7, Table X1.1)
Specific heat (J/kg K)	560	Approximate value for Type 316 stainless steel at 400°C (Ref. D4.1.25, Table 8)
Emissivity	0.8	Estimated value for stainless steel that has undergone some oxidation
Initial temperature (K)	513	Initial temperature upon removal from the cask. Estimated from <i>Thermal Responses of TAD and 5-DHLW/DOE SNF Waste Packages to a Hypothetical Fire Accident</i> (Ref. D4.1.25, Figure 1)
<b>Fuel Properties</b>		
Heated mass (kg)	9,700	Calculated based on thermal penetration depth (see text)
Specific heat (J/kg K)	438	Average for fuel region taken from <i>Thermal Responses of TAD and 5-DHLW/DOE SNF Waste Packages to a Hypothetical Fire Accident</i> (Ref. D4.1.25, Table 15)
Effective surface area (m <sup>2</sup> )	28.18	Projected area for radiation heat transfer. Calculated based on outer diameter of fuel region (1.67 m)
Emissivity	0.8	From <i>Thermal Responses of TAD and 5-DHLW/DOE SNF Waste Packages to a Hypothetical Fire Accident</i> (Ref. D4.1.25, Table 17)
Initial temperature (K)	543	Estimated from <i>Thermal Responses of TAD and 5-DHLW/DOE SNF Waste Packages to a Hypothetical Fire Accident</i> (Ref. D4.1.25, Figure 1)
<b>Post-Fire Conditions</b>		
Ambient temperature (K)	361	Post-fire temperature of 190°F - a value 100°F higher than the maximum interior facility temperature (Ref. D4.1.16, Section 3.2)
Heat transfer coefficient (W/m <sup>2</sup> K)	2.0	Approximate value based on correlations in (Ref. D4.1.41, pp. 456-457) (Results not sensitive to this value)

NOTE: SFC = spent fuel canister; SNF = spent nuclear fuel; TAD = transportation, aging, and disposal.

Source: Original

Table D2.1-5. Model Inputs – Canister in a Waste Package

Model Parameter	Value	Basis/Rationale
<b>Canister Properties</b>		
Outer diameter (m)	1.68	Minimum diameter listed in <i>Transportation, Aging and Disposal Canister System Performance Specification</i> (Ref. D4.1.28, Section 3.1.1)
Wall thickness (m)	0.0127 or 0.0254	0.5 inches is the thinnest canister wall thickness listed for current transport cask designs 1.0 inch is the anticipated TAD canister thickness and is also the thickness of the naval SFC
Length (m)	5.4	Typical length of TAD canister listed in <i>Transportation, Aging and Disposal Canister System Performance Specification</i> (Ref. D4.1.28, Section 3.1.1)
Density (kg/m <sup>3</sup> )	7980	Density of Type 316 stainless steel (Ref. D4.1.7, Table X1.1)
Specific heat (J/kg K)	560	Approximate value for Type 316 stainless steel at 400°C (Ref. D4.1.25, Table 8)
Emissivity	0.62	Average value for Type 316 stainless steel in <i>Mark's Standard Handbook for Mechanical Engineers</i> (Ref. D4.1.8, Table 4.3.2)
Initial temperature (K)	513	From <i>Thermal Responses of TAD and 5-DHLW/DOE SNF Waste Packages to a Hypothetical Fire Accident</i> (Ref. D4.1.25, Figure 1)
<b>Outer Barrier of Waste Package</b>		
Outer diameter (m)	1.8816	Listed in <i>TAD Waste Package Configuration</i> (Ref. D4.1.22), (Ref. D4.1.23), and (Ref. D4.1.24)
Wall thickness (m)	0.0254	Listed in <i>TAD Waste Package Configuration</i> (Ref. D4.1.22), (Ref. D4.1.23), and (Ref. D4.1.24)
Length (m)	5.4	Heated length adjacent to the TAD canister – same as TAD canister length
Density (kg/m <sup>3</sup> )	8690	Value for Alloy 22 (Ref. D4.1.5, Section II, Part B, SB-575, Section 7.1)
Specific heat (J/kg K)	476	Value for Alloy 22 at 400°C (Ref. D4.1.36, p. 13)
Emissivity	0.87	Value for Alloy 22 (Ref. D4.1.45, p. 10-297)
Initial temperature (K)	433	From <i>Thermal Responses of TAD and 5-DHLW/DOE SNF Waste Packages to a Hypothetical Fire Accident</i> (Ref. D4.1.25, Figure 1)
<b>Inner Barrier of Waste Package</b>		
Outer diameter (m)	1.8212	Listed in <i>TAD Waste Package Configuration</i> (Ref. D4.1.22), (Ref. D4.1.23), and (Ref. D4.1.24)
Wall Thickness (m)	0.0508	Listed in <i>TAD Waste Package Configuration</i> (Ref. D4.1.22), (Ref. D4.1.23), and (Ref. D4.1.24)
Length (m)	5.4	Heated length adjacent to the TAD canister – same as TAD canister length
Specific heat (J/kg K)	560	Approximate value for Type 316 stainless steel at 400°C (Ref. D4.1.25, Table 8)
Emissivity	0.62	Average value for Type 316 stainless steel in <i>Mark's Standard Handbook for Mechanical Engineers</i> (Ref. D4.1.8, Table 4.3.2)

Table D2.1-5. Model Inputs – Canister in a Waste Package (Continued)

Model Parameter	Value	Basis/Rationale
Initial temperature (K)	478	From <i>Thermal Responses of TAD and 5-DHLW/DOE SNF Waste Packages to a Hypothetical Fire Accident</i> (Ref. D4.1.25, Figure 1)
<b>Post-Fire Conditions</b>		
Ambient temperature (K)	361	Post-fire temperature of 190°F - a value 100°F higher than the maximum interior facility temperature (Ref. D4.1.16, Section 3.2)
Heat transfer coefficient (W/m <sup>2</sup> K)	2.0	Approximate value based on correlations in <i>Introduction to Heat Transfer</i> (Ref. D4.1.41, pp. 456-457) (Results not sensitive to this value)

NOTE: SFC = spent fuel canister; SNF = spent nuclear fuel; TAD = transportation, aging, and disposal.

Source: Original

Table D2.1-6. Model Inputs – Canister in Transportation Cask

Model Parameter	Value	Basis/Rationale
<b>Canister Properties</b>		
Outer diameter (m)	1.68	Minimum diameter listed in <i>Transportation, Aging and Disposal Canister System Performance Specification</i> (Ref. D4.1.28, Section 3.1.1)
Wall thickness (m)	0.0127 or 0.0254	0.5 inches is the thinnest canister wall thickness listed for current transport cask designs 1.0 inch is the anticipated TAD canister thickness and is also the thickness of the naval SFC
Length (m)	5.4	Typical length of TAD canister listed in <i>Transportation, Aging and Disposal Canister System Performance Specification</i> (Ref. D4.1.28, Section 3.1.1)
Density (kg/m <sup>3</sup> )	7980	Density of Type 316 stainless steel (Ref. D4.1.7, Table X1.1)
Specific heat (J/kg K)	560	Approximate value for Type 316 stainless steel at 400°C (Ref. D4.1.25, Table 8)
Emissivity	0.62	Average value for Type 316 stainless steel in <i>Mark's Standard Handbook for Mechanical Engineers</i> (Ref. D4.1.8, Table 4.3.2)
Initial temperature (K)	513	From <i>Thermal Responses of TAD and 5-DHLW/DOE SNF Waste Packages to a Hypothetical Fire Accident</i> (Ref. D4.1.25, Figure 1)
<b>Transportation Cask Outer Shell</b>		
Outer diameter (m)	2.438	From HI-STAR Transportation Cask SAR (Ref. D4.1.38, p. 1.2-3)
Wall thickness (m)	0.0127	Minimum outer shell thickness listed in cask SARs
Length (m)	5.4	Length adjacent to the TAD canister
Density (kg/m <sup>3</sup> )	7850	Density of 516 carbon steel (Ref. D4.1.6, Section II, Part A, SA-20, 14.1)
Specific heat (J/kg K)	604	Approximate value for 516 carbon steel at 400°C (Ref. D4.1.25, Table 10)

Table D2.1-6. Model Inputs – Canister in Transportation Cask (Continued)

Model Parameter	Value	Basis/Rationale
Emissivity	0.8	Average value for carbon steel in <i>Mark's Standard Handbook for Mechanical Engineers</i> (Ref. D4.1.8, Table 4.3.2)
Initial temperature (K)	381	Initial temperature in HI-STAR SAR (Ref. D4.1.38, Figure 3.5.3)
<b>Transportation Cask Gamma Shield</b>		
Outer diameter (m)	2.148	From HI-STAR Transportation Cask SAR (Ref. D4.1.38, Drawing No.3913)
Wall thickness (m)	0.19	A lower value for the combined thickness of gamma shield and inner containment listed in cask SARs
Length (m)	5.4	Length adjacent to the TAD canister
Density (kg/m <sup>3</sup> )	7850	Density of 516 carbon steel (Ref. D4.1.6, Section II, Part A, SA-20, 14.1)
Specific heat (J/kg K)	604	Approximate value for 516 carbon steel at 400°C (Ref. D4.1.25, Table 10)
Emissivity	0.8	Average value for carbon steel in <i>Mark's Standard Handbook for Mechanical Engineers</i> (Ref. D4.1.8, Table 4.3.2)
Initial temperature (K)	405	Approximate average initial temperature in HI-STAR SAR (Ref. D4.1.38, Figure 3.5.3)
Ambient temperature (K)	361	Post-fire temperature of 190°F - a value 100°F higher than the maximum interior facility temperature (Ref. D4.1.16, Section 3.2)
Heat transfer coefficient (W/m <sup>2</sup> K)	2.0	Approximate value based on correlations in <i>Introduction to Heat Transfer</i> (Ref. D4.1.41, pp. 456-457) (Results not sensitive to this value)

NOTE: SAR = Safety Analysis Report; SFC = spent fuel canister; SNF = spent nuclear fuel; TAD = transportation, aging, and disposal.

Source: Original

Table D2.1-7. Model Inputs – Canister in a Shielded Bell

Model Parameter	Value	Basis/Rationale
<b>Canister Properties</b>		
Outer diameter (m)	1.68	Minimum diameter listed in <i>Transportation, Aging and Disposal Canister System Performance Specification</i> (Ref. D4.1.28, Section 3.1.1)
Wall thickness (m)	0.0127 or 0.0254	0.5 inches is the thinnest canister wall thickness listed for current transport cask designs 1.0 inch is the anticipated TAD canister thickness and is also the thickness of the naval SFC
Length (m)	5.4	Typical length of TAD canister listed in <i>Transportation, Aging and Disposal Canister System Performance Specification</i> (Ref. D4.1.28, Section 3.1.1)
Density (kg/m <sup>3</sup> )	7980	Density of Type 316 stainless steel (Ref. D4.1.7, Table X1.1)
Specific heat (J/kg K)	560	Approximate value for Type 316 stainless steel at 400°C (Ref. D4.1.25, Table 8)
Emissivity	0.62	Average value for Type 316 stainless steel in <i>Mark's Standard Handbook for Mechanical Engineers</i> (Ref. D4.1.8, Table 4.3.2)
Initial temperature (K)	513	From <i>Thermal Responses of TAD and 5-DHLW/DOE SNF Waste Packages to a Hypothetical Fire Accident</i> (Ref. D4.1.25, Figure 1)
<b>Shielded Bell</b>		
Outer diameter (m)	2.388	From <i>CRCF, IHF, RF, and WHF Canister Transfer Machine Mechanical Equipment Envelope</i> (Ref. D4.1.11)
Wall thickness (m)	0.273	From <i>CRCF, IHF, RF, and WHF Canister Transfer Machine Mechanical Equipment Envelope</i> (Ref. D4.1.11)
Length (m)	7.62	From <i>CRCF, IHF, RF, and WHF Canister Transfer Machine Mechanical Equipment Envelope</i> (Ref. D4.1.11)
Density (kg/m <sup>3</sup> )	7980	Density of Type 316 stainless steel (Ref. D4.1.7, Table X1.1)
Specific heat (J/kg K)	560	Approximate value for Type 316 stainless steel at 400°C (Ref. D4.1.25, Table 8)
Emissivity	0.67	Approximate value at elevated temperature (corresponds to little oxidation of the surface)
Initial temperature (K)	306	Maximum interior facility temperature of 90°F (Ref. D4.1.16, Section 3.2)
<b>Post-Fire Conditions</b>		
Ambient temperature (K)	367	Post-fire temperature of 190°F - a value 100°F higher than the maximum operating temperature listed above
Heat transfer coefficient (W/m <sup>2</sup> K)	2.0	Approximate value based on correlations in <i>Introduction to Heat Transfer</i> (Ref. D4.1.41, pp. 456-457) (Results not sensitive to this value)

NOTE: SFC = spent fuel canister; SNF = spent nuclear fuel; TAD = transportation, aging, and disposal.

Source: Original

### D2.1.4.5 Uncertainty in Canister Failure Temperature

Using the models discussed in Sections D2.1.4.1 and D2.1.4.2, the temperature increase of a canister due to a fire can be calculated. In order to determine whether the temperature is sufficient to cause the canister to fail, it is necessary to determine the canister temperature at which failure would occur. Two failure modes were considered:

1. *Creep-Induced Failure.* Creep is the plastic deformation that takes place when a material is held at high temperature for an extended period under tensile load. This mode of failure is possible for long duration fires.
2. *Limit Load Failure.* This failure mode occurs when the load exerted on a material exceeds its structural strength. As the temperature of the canister increases in temperature, its strength decreases. Failure is generally predicted at some fraction (usually around 70%) of the ultimate strength.

The modeling associated with these failure modes is described in the following subsections.

#### D2.1.4.5.1 Modeling Creep-Induced Failure

Creep failure could occur if the canister is maintained at a high temperature for a lengthy period of time. One way to predict creep failure is to calculate a creep damage index, which defines the ratio of the creep damage to the cumulative creep required for failure. Such a model has been used by researchers at Argonne National Laboratory to predict failure of steam generator tubes under accident conditions (Ref. D4.1.46). In the Argonne National Laboratory model, failure occurs when the creep damage index reaches a value of 1. Written in the form of an equation, this condition is given by:

$$\int_0^{t_f} \frac{dt}{t_R(T, \sigma)} = 1 \quad (\text{Eq. D-16})$$

where

- T = the temperature experienced by the canister (a function of time)  
 σ = the tensile stress exerted on the canister wall, and  
 t<sub>f</sub> = the canister failure time (the time at which the equality is satisfied).

The function in the denominator of Equation D-16 is

$$t_R = 10^{\frac{P_{LM}}{T} - 20} \quad (\text{Eq. D-17})$$

where P<sub>LM</sub> is the Larson-Miller parameter *Transactions of the American Society of Mechanical Engineers*, 74(Ref. D4.1.44), which is a material property of the canister material and is a function of the applied stress.

Since the canisters are pressurized to varying degrees with a combination of helium or air used to backfill the canister and gases released when the fuel fails, the pressure inside the canister will increase as the canister gets hotter. The internal pressure exerts a hoop stress in the radial direction that puts the canister wall under tension. It is this stress that controls failure of the canister wall. The hoop stress,  $\sigma$ , is calculated using the following equation:

$$\sigma = \frac{P r_c}{h} \quad (\text{Eq. D-18})$$

where

- h = the thickness of the canister wall
- $r_c$  = the mean radius of the canister
- P = the pressure difference across the canister wall.

#### D2.1.4.5.2 Modeling Limit Load Failure

Limit load failure occurs when the load on a structure exceeds its ability to withstand that load. As with the creep failure mode, the load on the canister wall is a hoop stress and is calculated using Equation D-18.

The capability of the canister to withstand a load is given by a flow stress, which is defined by (Ref. D4.1.46, p. 3):

$$\bar{\sigma} = k(\sigma_y + \sigma_u) \quad (\text{Eq. D-19})$$

where

- k = a multiplication factor (0.5 in the current analysis)
- $\sigma_y$  = the yield strength (temperature dependent)
- $\sigma_u$  = the ultimate strength (temperature dependent).

The yield and ultimate strength are both temperature-dependent properties, so the flow stress is also a temperature-dependent property. For a typical 316 stainless steel, a value of 0.5 for k yields a flow stress that is approximately 0.7 times the ultimate strength. Failure is predicted if the hoop stress exceeds the flow stress.

This failure condition is consistent with the failure condition outlined in *2004 ASME Boiler and Pressure Vessel Code* (Ref. D4.1.6, Appendix F, paragraph F-1331). The ASME code specifies that for ferritic steels, the primary membrane stress intensity shall not exceed  $0.7 \sigma_u$ . For austenitic steels, the primary membrane stress intensity shall not exceed the greater of  $0.7 \sigma_u$  or  $\sigma_y + (\sigma_u + \sigma_y)/3$ . As is noted below, for type 316 stainless steels,  $0.7 \sigma_u$  is always the controlling condition.

### D2.1.4.5.3 Inputs to the Canister Failure Models

The canister failure models require the following inputs:

- the value for the Larson-Miller parameter (a function of temperature and stress)
- the value for the flow stress (a function of temperature)
- the time-dependent internal pressure and temperature experienced by the canister.

The following discussion outlines how these values were determined.

#### D2.1.4.5.3.1 Larson-Miller Parameter

The value for the Larson-Miller parameter can be determined based on creep data provided by material suppliers. In the absence of data specific to the steels used for the spent fuel and HLW canisters to arrive at Yucca Mountain, a literature review was performed to obtain representative creep rupture data for steels of the type expected to be used.

The primary focus of this data search was type 316 stainless steel since that is the steel most likely to be used for the spent fuel or HLW canisters. Data were collected from the following sources:

- “Properties and Selection of Metals.” Volume 1 of *Metals Handbook* (Ref. D4.1.3).
- Reliability and Longevity of Furnace Components as Influenced by Alloy of Construction. H-3124 (Ref. D4.1.35).
- *Creep of the Austenitic Steel AISI 316L(N) -Experiments and Models* (Ref. D4.1.58).
- “Assessment of Creep Behaviour of Austenitic Stainless Steel Welds.” *Creep-Fatigue Damage Rules for Advanced Fast Reactor Design, Proceedings of a Technical Committee Meeting, Manchester, United Kingdom, 11-13 June 1996* (Ref. D4.1.59).
- *Materials Selection for High Temperature Applications [TKK-MTR-4/05]* (Ref. D4.1.60).

The creep data provides the time required for creep rupture given a specified constant temperature and applied tensile stress.

Using this data, the value for the Larson-Miller parameter (Ref. D4.1.44) can be determined from the following equation:

$$P_{LM} = T[C + \log(t_f)] \quad (\text{Eq. D-20})$$

where

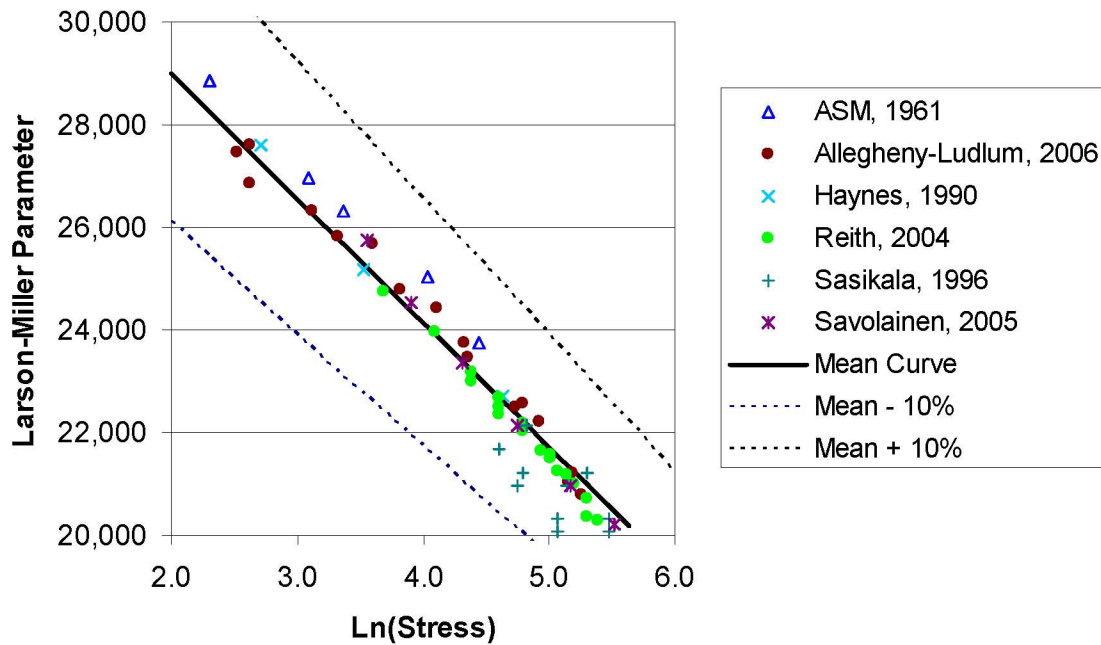
T	=	temperature (K)
$t_f$	=	failure time (hours) determined in testing
C	=	a constant that is approximately 20 for most stainless steels

Using this equation and the data collected in the literature review, values for the Larson-Miller parameter were calculated. The calculated values for the Larson-Miller parameter are shown in Figure D2.1-2. As shown in the figure, the Larson-Miller parameter decreases as the applied stress increases.

In order to apply the results shown in the table outside the range of stresses considered in the table, it is necessary to determine a correlation that best fits the data. The best-fit curve, which is also plotted in Figure D2.1-2, is given by the following equation:

$$P_{LM} = 33,845 - 2,423 \ln(\sigma) \quad (\text{Eq. D-21})$$

As shown in Figure D2.1-2, the value for the Larson-Miller parameter varies from one metal specimen to the next and from one vendor to the next. This variability is illustrated, in part, by the variability in the data shown in the figure. In addition, the research by Sasikala, et al. (Ref. D4.1.59) showed that stainless steel weld material is generally less creep-resistant than the base metal (this is illustrated by the five outlier points on the figure which were determined for the weld material rather than the base metal). The variability in the Larson-Miller parameter must be reflected in the uncertainty analysis for the canister failure temperature.



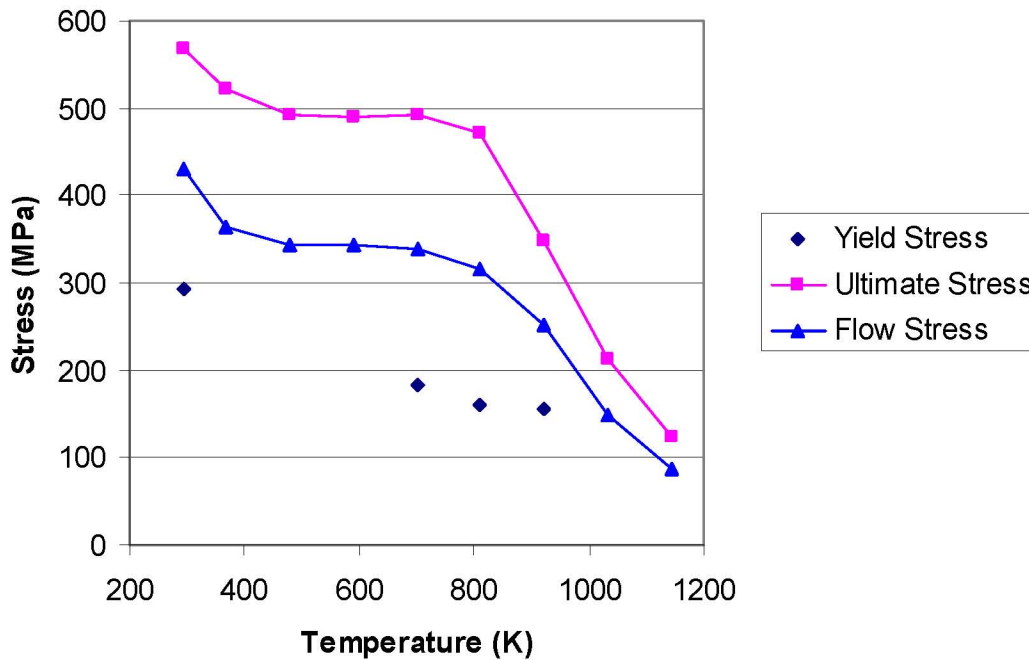
Source: Excel Spreadsheet *Creep rupture - Fast Heatup 1 inch.xls* found in Attachment H

Figure D2.1-2. Plot of Larson-Miller Parameter for Type 316 Stainless Steel

The uncertainty in the Larson-Miller parameter is treated within the canister failure analysis by multiplying the calculated value for  $P_{LM}$  by a factor  $(1+a)$ , where the value for  $a$  is normally distributed with a mean of 0.0 and a standard deviation of 0.038. Using this formulation, 99% of all canister steels would have  $P_{LM}$  values within approximately 10% of the calculated value. This uncertainty is believed to reflect the variability between different canister steels as well as the variability between the base metal and the weld material.

#### D2.1.4.5.3.2 Flow Stress

In the canister failure analysis, the flow stress is the average of the yield and ultimate strength. Both the yield and ultimate strength are temperature-dependent and decrease rapidly above a temperature of about 800 K. Figure D2.1-3 presents typical curves for the yield and ultimate strength of Type 316 stainless steel as a function of temperature (Ref. D4.1.1). The figure also presents the calculated flow stress curve. For temperatures with no yield strength data, the flow stress equals 0.7 times the ultimate strength.



Source: Original

Figure D2.1-3. Yield, Ultimate, and Flow Stress for Type 316 Stainless Steel

For the temperature range of interest, the flow stress curve can be fit to two straight lines: one line for temperatures between 350 K and 800 K and another for temperatures above 800 K. The equations for these two lines are provided below:

$$\bar{\sigma} = 395.9 - 0.0925T \quad \text{for } T < 800 \text{ K} \quad (R^2 = 0.889) \quad (\text{Eq. D-22a})$$

$$\bar{\sigma} = 899.1 - 0.7139T \quad \text{for } T \geq 800 \text{ K} \quad (R^2 = 0.989) \quad (\text{Eq. D-22b})$$

Note that the fit is particularly good for the upper temperature range, which is of greatest interest in the current analysis.

As with the value for the Larson-Miller parameter, the value for the flow stress is uncertain. The uncertainty in the flow stress was treated in the same manner as the uncertainty in the Larson-Miller parameter. Specifically, the mean value described by the equations provided above was multiplied by a factor  $(1 + a)$  where the value for  $a$  is normally distributed with a standard deviation of 0.038. This distribution results in 99% of all canister steels having a flow stress within 10% of the mean value given by the equations. This adequately reflects the variability in the material properties of Type 316 steels, the variability between the properties of the base metal and weld material, and the potential for other types of steel with lower or higher tensile strength to be used in manufacture of the canisters.

### D2.1.4.5.3.3 Pressure Difference and Temperature Histories

Creep failure and limit load failure depend on the time-dependent internal pressure and canister temperature. The canister temperature depends on the fire severity and also on whether the canister is bare or enclosed in a waste package or cask. The canister temperature is calculated using a separate analysis, as discussed above. Rather than attempting to couple the canister failure and canister heatup analyses into a single calculation, a separate canister failure analysis was completed. This analysis required the following inputs: the rate of temperature increase of the canister wall and the relationship between the internal canister pressure and the temperature of the canister wall.

Based on a series of runs with the canister heat transfer models discussed above, it was determined that the rate of temperature increase for a bare canister was likely to range from a low of around 25 K/min to a high of around 175 K/min. This range was input as a normal distribution with a mean of 100 K/min and a standard deviation of 25 K/min. Similar runs for the non-bare canister cases indicated a much slower heatup rate. For these cases, the canister heatup rate was input as a normal distribution with a mean of 10 K/min and a standard deviation of 2.5 K/min.

Analyses with a special version of the bare canister heat transfer model were also used to characterize the rate at which the temperature of the gas inside the canister would increase as a result of heating of the canister wall. This version of the model included convective heat transfer from the canister wall to the gas, from the canister wall to fuel assemblies inside the canister, and from the fuel assemblies to the gas inside the canister. These analyses showed a substantial lag in temperature between the canister wall and the gas.

The following equation was used to calculate the internal pressure of the canister based on the canister temperature:

$$P = P_0 \left[ 1 + C \left( \frac{T_{\text{can}} - T_{\text{can},0}}{T_{\text{can},0}} \right) \right] \quad (\text{Eq. D-23})$$

where

- $P_0$  = initial pressure inside the canister (including potential fuel failures)
- $T_{\text{can},0}$  = initial temperature of the canister wall
- $T_{\text{can}}$  = canister temperature at the current timestep
- $C$  = a constant that depends on the canister heating rate.

Note that if the value for  $C$  is set equal to 1.0 in this equation, the proportional change in pressure is equal to the proportional change in temperature. This would be true if the gas and canister temperatures increased at the same rate. Because the gas temperature lags behind the canister temperature, the value for  $C$  is always less than 1. Rather than attempting to model the variability in the value for  $C$ , the analysis used a bounding value of 0.5 for all analyses. This value bounded the range of values calculated in the separate heat transfer analysis.

The initial pressure,  $P_0$ , in Equation D-23 varies over a wide range depending on the amount of overpressure supplied when the canister is sealed, the extent of fuel rod failures, and the type of fuel stored in the canister. Since the canister failure analysis considers only the increase in gas temperature due to the fire, the initial pressure must reflect potential fuel failures during the fire.

The SARs prepared by transportation cask vendors were consulted for information on internal pressure under normal and accident conditions (see for example, Section 3.6.6 of *GA-9 Legal Weight Truck From-Reactor Spent Fuel Shipping Cask, Final Design Report* (Ref. D4.1.34)). The SARs provide information on the initial overpressure in the canister and the pressure increase associated with fuel rod failures. Based on this information, an uncertainty distribution for the initial pressure in the canister was developed. The uncertainty is characterized by a Weibull distribution with a minimum of 5 psig, a scale factor of 45 psig, and a shape factor of 2.4. This distribution is applied to all canisters considered in the PCSA.

### **D2.1.5 Probabilistic Fragility Analysis**

The mechanistic models described above produce results that are deterministic. That is, for a given set of input values, they yield a single answer. However, as has been shown, the inputs to the models are uncertain. Uncertainty in the input parameters could lead to a substantial variation in the predicted canister thermal response and failure temperature. Therefore, it is necessary to treat the analysis in a probabilistic manner. It is in the fragility analysis that all the parameters that affect the failure of the spent fuel or HLW canister are addressed in a probabilistic fashion.

The fragility analysis consists of two separate probabilistic analyses: (1) an analysis to determine the probability distribution for the canister failure temperature, and (2) an analysis to determine the maximum temperature reached by the canister due to the fire. These two analyses are combined to determine the probability that the canister fails as a result of the fire.

Calculations were performed for canisters inside a waste package, a cask, or a shielded bell. As discussed earlier, two canister wall thicknesses were evaluated: 0.5 inches (hereafter referred to as *thin-walled* canisters) and 1.0 inch (hereafter referred to as *thick-walled* canisters). The following sections describe how these analyses are performed and present the calculated failure probabilities for the various canister configurations of interest.

#### **D2.1.5.1 Probabilistic Analysis of Canister Failure Temperature**

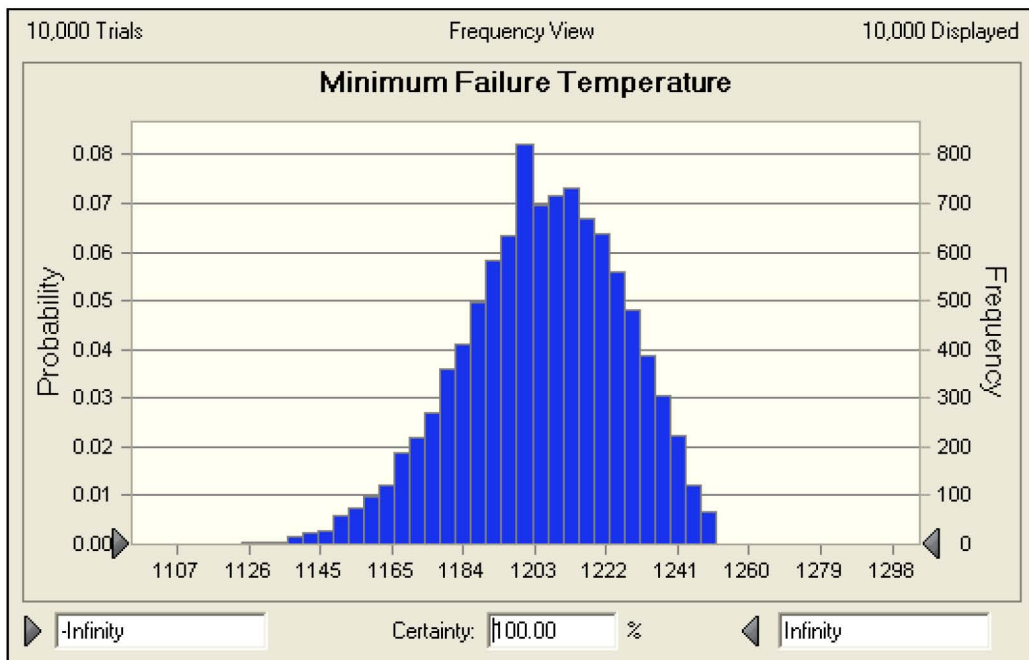
The first step in the fragility analysis was to determine the probability distribution for the canister failure temperature. The probability distribution was determined using a Monte Carlo analysis in which the failure models outlined in Section D2.1.4 were repeatedly solved with parameter values sampled from the uncertainty distributions discussed in that section. The failure temperature for each sample was the lower of the two temperatures calculated based on creep rupture or limit load failure.

A Microsoft Excel add-in product, Crystal Ball, was used to perform Monte Carlo simulation. Latin hypercube sampling was used to ensure that parameter samples represented the assigned distributions adequately.

Figure D2.1-4 shows the calculated canister failure temperature distribution for canisters inside a waste package, transportation cask, or shielded bell. This calculation used the lower heating rate discussed in Section D2.1.4.5.3.3. The probability distribution shown in Figure D2.1-4 is well-characterized by a normal distribution with a mean of 1,203 K and a standard deviation of 22.85 K. This normal distribution provides a particularly good fit to the lower failure temperature portion of the distribution which is the most important for the canister failure analysis.

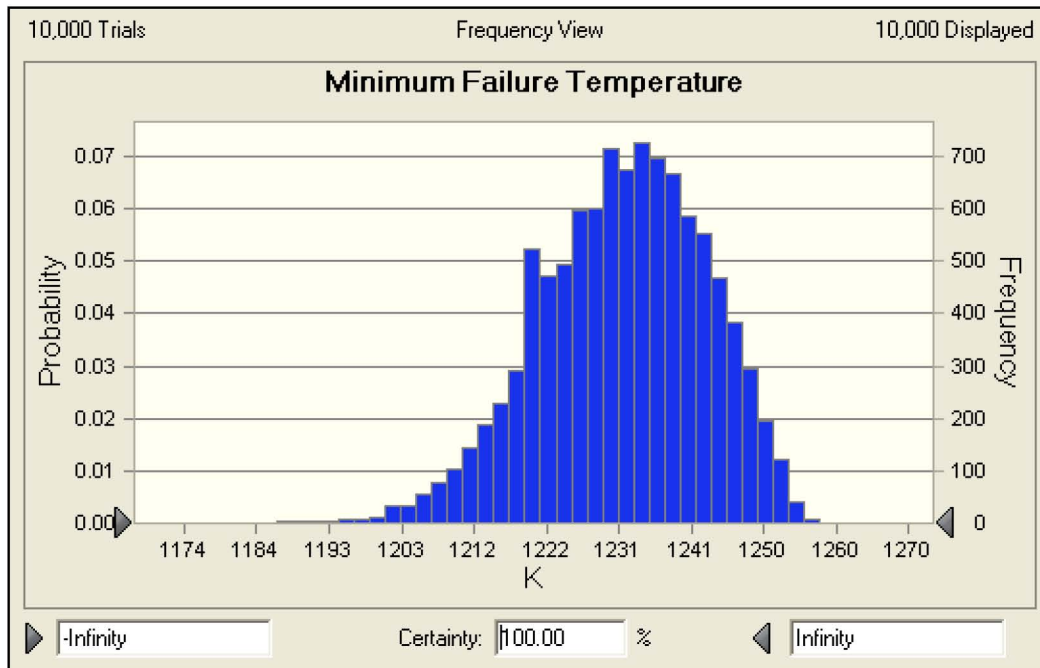
A similar analysis was performed for bare canisters. This calculation used the higher heating rate discussed in Section D2.1.4.5.3.3. The resulting probability distribution was nearly identical to the one shown in Figure D2.1-4. The reason for this is that canister failure was nearly always due to limit load failure rather than creep failure, so the difference in heating rates for the two configurations was not important.

A similar analysis was performed for thick-walled canisters. As with the thin-walled canisters, the probability distribution for the canister failure temperature was found to be nearly independent of the canister heating rate. Figure D2.1-5 shows the calculated probability distribution. This probability distribution is well-characterized by a normal distribution with a mean of 1,232 K and a standard deviation of 12.3 K. This normal distribution provides a particularly good fit to the lower failure temperature portion of the distribution which is the most important for the canister failure analysis.



Source: Original

Figure D2.1-4. Probability Distribution for the Failure Temperature of Thin-Walled Canisters



Source: Original

Figure D2.1-5. Probability Distribution for the Failure Temperature of Thick-Walled Canisters

### D2.1.5.2 Probabilistic Analysis to Determine the Maximum Canister Temperature and Canister Failure Probability

The next step in the fragility analysis was to determine the maximum temperature of the canister as a result of the fire. In this analysis, Monte Carlo techniques were used to repeatedly sample from the uncertainty distributions discussed in Section D2.1.4 while applying the canister heating models to determine the maximum temperature of the canister due to the fire. As with the failure temperature analysis, Crystal Ball was used to perform the Monte Carlo simulation.

For each Monte Carlo sample, the calculated maximum canister temperature was then compared to a canister failure temperature sampled from the probability distribution discussed in Section D2.1.5.1. The canister is considered failed if the maximum temperature of the canister exceeded the sampled failure temperature for that Monte Carlo sample. The failure probability was determined as the fraction of the samples for which failure was calculated.

This process was repeated for a sufficient number of samples to provide a good statistical basis for the failure probability. The rule of thumb used in determining the required number of samples was that at least 10 failures had to be calculated. Thus, if the failure probability was on the order of  $10^{-4}$ , 100,000 ( $10^5$ ) samples were needed. The maximum number of samples for any run was set at 1 million. If no failures were calculated for one million samples, the failure probability was recorded as being less than  $10^{-6}$ .

Since each Monte Carlo sample has two possible outcomes (failure or no failure), each sample represents a Bernoulli trial. Since the probability of failure or no failure is the same for each trial, the outcome from the sampling process can be represented by a binomial distribution. The

binomial distribution is closely approximated by a normal distribution if the number of failures is greater than about five. The mean of the normal distribution is simply the number of failures divided by the total number of samples. The standard deviation of the normal distribution is given by the following equation:

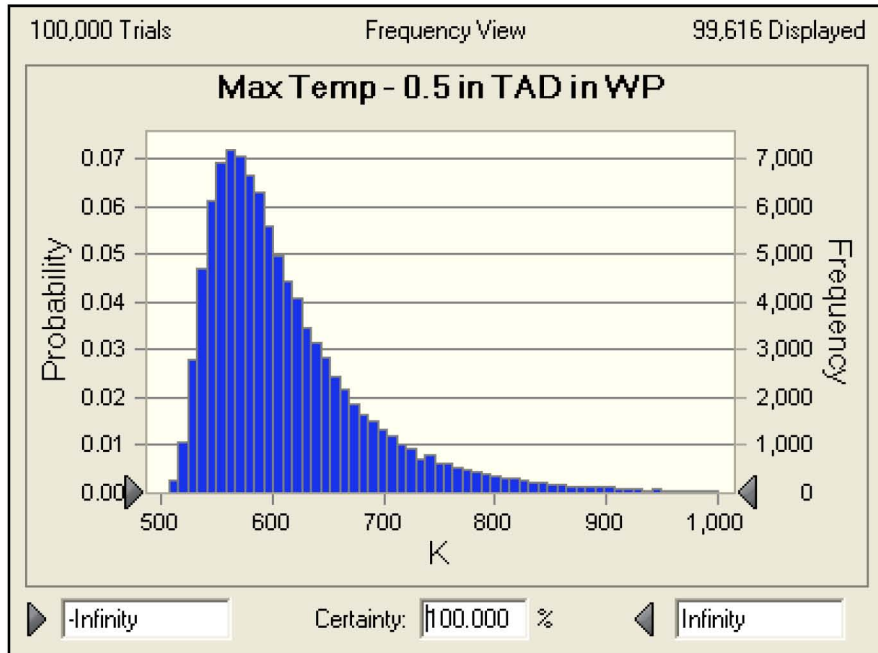
$$\sigma = \sqrt{\frac{\frac{n_{\text{fail}}}{N} \left( \frac{N - n_{\text{fail}}}{N} \right)}{N}} \quad (\text{Eq. D-24})$$

where  $n_{\text{fail}}$  is the number of failures,  $N$  is the total number of Monte Carlo samples, and  $p_{\text{fail}}$  is the calculated mean failure probability ( $n_{\text{fail}}/N$ ).

Figure D2.1-6 shows the calculated distribution for the maximum temperature reached by a thin-walled canister inside a waste package. The figure shows that the vast majority of the Monte Carlo samples had maximum temperatures well below 950 K. Only under extreme combinations of fire temperature and duration did the calculated maximum temperature approach the failure temperatures shown in Figure D2.1-4. Consequently there were only 32 calculated canister failures out of a total of 100,000 Monte Carlo samples. The resulting mean value for the canister failure probability is therefore  $32/100,000$  or  $3.2 \times 10^{-4}$ . The standard deviation calculated using Equation D-24 is  $5.7 \times 10^{-5}$ . The mean and standard deviation of the failure probability are shown in Table D2.1-8.

A similar analysis was performed for a thick-walled canister inside a waste package. Because of the thicker wall, the failure temperature of the canister is higher than for the thin-walled canister. In addition, the thick-walled canister heats up more slowly than the thin-walled canister because of its greater mass. These two factors combine to substantially lower the probability of failure for these canisters. In the Monte Carlo analysis, 20 failures were calculated for 200,000 samples, which results in a mean failure probability of  $1 \times 10^{-4}$  and a standard deviation of  $2.2 \times 10^{-5}$ .

Similar calculations have been performed for a canister inside a transportation cask and a canister inside the shielded bell of the CTM. The resulting mean and standard deviation for the canister failure probability are provided in Table D2.1-8.



Source: Original

Figure D2.1-6. Probability Distribution for Maximum Canister Temperature – Thin-Walled Canister in a Waste Package

Table D2.1-8. Summary of Canister Failure Probabilities in Fire

Configuration <sup>b</sup>	Monte Carlo Results		Failure Probability	
	Total Failures	Total Trials	Mean	Standard Deviation
Thin-walled canister in a waste package <sup>a</sup>	32	100,000	$3.2 \times 10^{-4}$	$5.7 \times 10^{-5}$
Thick-walled canister in a waste package <sup>a</sup>	20	200,000	$1.0 \times 10^{-4}$	$2.2 \times 10^{-5}$
Thin-walled canister in a transport cask	2	1,000,000	$2.0 \times 10^{-6}$	$1.4 \times 10^{-6}$
Thick-walled canister in a transport cask	1	1,000,000	$1.0 \times 10^{-6}$	$1.0 \times 10^{-6}$
Thin-walled canister in a shielded bell	27	200,000	$1.4 \times 10^{-4}$	$2.6 \times 10^{-5}$
Thick-walled canister in a shielded bell	27	300,000	$9.0 \times 10^{-5}$	$1.7 \times 10^{-5}$

NOTE: <sup>a</sup>For the 5-DHLW/DOE SNF waste package, this probability applies only to the DOE HLW canisters located on the periphery of the waste package. The DOE SNF canister in center of the waste package would not be heated appreciably by the fire.

<sup>b</sup>Configurations not addressed in this table include any canister in a waste package that is inside the transfer trolley or any canister inside an aging overpack. In these configurations, the canister is protected from the fire by the massive steel transfer trolley or by the massive concrete overpack. Calculations have shown that the temperatures experienced by the canister in these configurations are well below the canister failure temperature. Although failures for these configurations could be screened on this basis, a conservative screening probability of  $1 \times 10^{-6}$  is used in the PCSA.

Source: Original

Note that Table D2.1-8 contains no failure probability for a bare canister configuration. The reason for this is that the canister is outside of a waste package or cask for only a short time. During that time, the canister is usually inside the shielded bell of the CTM. The preceding analysis addressed a fire outside the shielded bell. When in that configuration, the canister is shielded from the direct effects of the fire. A fire inside the shielded bell, which could directly heat the canister, was not considered to be physically realizable for two reasons. First, the hydraulic fluid used in the CTM equipment is non-flammable (Ref. D4.1.48, p 30) and no other combustible material could be present inside the bell to cause a fire. Second, the annular gap between the canister and the bell only three inches wide, but is approximately 27 feet long. Given this configuration, it is unlikely that there would be sufficient inflow of air to sustain a large fire. There may be sufficient inflow to sustain a localized fire, but such a fire would not be adequate to heat the canister to failure.

The canister is also outside of a cask, waste package, or shielded bell as it is being moved from a cask into the shielded bell or from the shielded bell into a waste package. The time during which the canister would be in this configuration is extremely short (a matter of minutes) so a fire that occurs during this time is extremely unlikely. In addition, because the gap between the top of the waste package or cask and ceiling of the transfer cell is generally much shorter than the height of the canister, only a small portion of the canister surface would be exposed to the fire. Furthermore, this exposure would only be for the short time that the canister was in motion.

For these reasons, failure of a bare canister was not considered a physically realizable threat to breach of a canister and was not treated further.

The notes to Table D2.1-8 mention two other configurations for which fire-induced canister failure is not credible: a fire outside a waste package inside a waste package transfer trolley (WPTT) and a fire outside an aging overpack. These two special cases are discussed below.

The failure probability for a waste package in the WPTT was determined using the probabilistic methodology discussed above. For this calculation, the waste package calculation discussed earlier was modified by simply adding a thermal barrier outside the waste package to represent the WPTT. The fire heats the WPTT which then transfers heat by radiation to the outer barrier of the waste package. The WPTT was modeled as having an equivalent external diameter of 3.05 m, a thickness of 20.3 cm (steel thickness only<sup>1</sup>), and a mass of 89,000 kg. The transfer trolley was considered to be made of a stainless steel with an average specific heat of 476 J/kg K. The probabilistic analysis was run for 1 million Monte Carlo samples and no failures were calculated. Though the maximum temperature calculated in this analysis was well below the failure temperatures shown in Figures D2.1-4 and D2.1-5, a conservative failure probability of  $1 \times 10^{-6}$  is used in the PCSA.

The probabilistic methodology discussed above could not be used for analysis of canister failure for a fire outside an aging overpack. The reason for this is that the concrete that comprises the majority of the aging overpack has a very low thermal conductivity. Therefore, the underlying premise of a relatively uniform temperature in each cylindrical region would be incorrect. Instead, a simple heat conduction calculation was performed to determine how far into the concrete heat could be conducted during a fire. The thermal penetration depth (from Equation D-11) was estimated based on a bounding 2-hour fire and concrete with the following average properties: thermal conductivity = 1.2 W/m K; density = 2,200 kg/m<sup>3</sup>; and specific heat = 1,000 J/kg K. The thermal penetration depth calculated for these conditions was 6.3 cm. Since the aging overpack is expected to be at least 24 inches (61 cm) thick, the canister inside the aging overpack will not be heated significantly by the fire. A conservative failure probability of  $1 \times 10^{-6}$  is used in the PCSA.

Note that, in this calculation, the fire was modeled as being only on the outside of the aging overpack. Though the overpack has ventilation openings for natural circulation, this flow path is expected to provide sufficient resistance to airflow that (1) combustion could not be sustained inside the overpack even if fuel entered through the openings, and (2) hot gases would likely flow over the outer surface of the overpack rather than enter the ventilation openings and flow up through the annulus inside the overpack. In fact, because oxygen would be consumed by the fire near the bottom of the overpack, air may actually flow downward through the ventilation openings to supply air to the fire.

### **D2.1.5.3 Analysis to Determine Failure Probabilities for Bare Fuel in Casks Exposed to Fire**

Another fire-induced failure mode is of interest in the PCSA; namely, failure of a transport cask containing bare spent fuel assemblies. The analysis uses GA-4/GA-9 transportation casks to represent casks of this type. Should a transportation cask containing uncanistered spent nuclear fuel fail in a fire, it is of interest for determining the source term to know if the fuel cladding is heated above its failure temperature (approximately 700°C to 800°C).

---

<sup>1</sup> There is also a 7.5-inch layer of borated polyethylene. Because this layer is likely to melt early in the fire transient, it is ignored in the analysis.

A modified version of the model for failure of a canister in a transportation cask was used to determine the probability that fuel will exceed this failure temperature. In the modified spreadsheet, the canister was replaced by the mass of fuel that would be heated during the fire. As in the bare canister analysis discussed in Section D2.1.4.1, this mass was estimated based on the calculated thermal penetration depth. Based on the information provided in the GA-9 SAR report (Ref. D4.1.34, p. 3.6-3), the following average spent fuel properties were determined: thermal conductivity = 1.5 W/m K, density  $\times$  specific heat =  $9.9 \times 10^5$  J/m<sup>3</sup> K. For a 1-hour fire, the calculated thermal penetration depth is 7.4 cm and the effective fuel mass is 1,910 kg. Since the severe fires of greatest concern have durations of 1 hour or longer, this fuel mass represents a reasonable, but probably conservative, estimate.

Other modifications to the model included changes to model the geometry and materials used in the GA-4/GA-9 casks. The inputs to the model are presented in Table D2.1-9. As in the previous analyses, the model does not rely on neutron shield because it is liable to melt early in the transient.

The model was run for three different fuel failure temperatures: 700°C, 750°C, and 800°C. This range of failure temperatures represents the lower end of the values reported in the literature (Ref. D4.1.65, pp. 7-20 to 7-21). As shown in Table D2.1-10, the calculated fuel failure probabilities were less than 0.001.

Table D2.1-9. Model Inputs – Bare Fuel Cask

Model Parameter	Value	Basis/Rationale
<b>Fuel Properties</b>		
Heated mass (kg)	1,910	Calculated based on thermal penetration depth (see text)
Specific heat (J/kg K)	438	Average for fuel region taken from <i>Thermal Responses of TAD and 5-DHLW/DOE SNL Waste Packages to a Hypothetical Fire Accident</i> (Ref. D4.1.25, Table 15)
Effective surface area (m <sup>2</sup> )	10.0	Projected area for radiation heat transfer. Calculated based on equivalent outer diameter of fuel region (0.66 m)
Emissivity	0.8	From <i>Thermal Responses of TAD and 5-DHLW/DOE SNL Waste Packages to a Hypothetical Fire Accident</i> (Ref. D4.1.25, Table 17)
Initial temperature (K)	400	Estimated from fig 3.4-4 in GA-9 SAR (Ref. D4.1.34)
<b>Transportation Cask Outer Shell</b>		
Outer diameter (m)	1.12	Equivalent diameter estimated based on GA-9 SAR (Ref. D4.1.34, Figure 1.2-9)
Wall thickness (m)	0.0032	Minimum outer shell thickness listed in cask SAR (Ref. D4.1.34)
Length (m)	4.25	Length adjacent to the fuel region
Density (kg/m <sup>3</sup> )	7850	Density of 516 carbon steel (Ref. D4.1.6, Section II, Part A, SA-20, 14.1)
Specific heat (J/kg K)	604	Approximate value for 516 carbon steel at 400°C (Ref. D4.1.25, Table 10)
Emissivity	0.8	Average value for carbon steel in Avallone and Baumeister, (Ref. D4.1.8, Table 4.3.2)
Initial temperature (K)	344	Estimated from fig 3.4-4 in GA-9 SAR (Ref. D4.1.34)

Table D2.1-9. Model Inputs – Bare Fuel Cask (Continued)

Model Parameter	Value	Basis/Rationale
<b>Transportation Cask Gamma Shield<sup>a</sup></b>		
Outer diameter (m)	0.902	Equivalent diameter estimated based on GA-9 SAR (Ref. D4.1.34, Figure 1.2-9)
Wall thickness (m)	0.107	Combined thickness of stainless steel and depleted uranium shields (steel: 0.0445 m; DU: 0.0622 m)(Ref. D4.1.34)
Length (m)	4.25	Length adjacent to the fuel region
Mass × specific heat (J/K)	$3.45 \times 10^6$	Based on calculated masses of steel and DU and specific heats listed in GA-9 SAR (Ref. D4.1.34, Tables 2.2-1 and 3.2-2)
Emissivity	0.8	Average value for carbon steel in Avallone and Baumeister, (Ref. D4.1.8, Table 4.3.2)
Initial temperature (K)	360	Estimated from fig 3.4-4 in GA-9 SAR (Ref. D4.1.34)
<b>Post-Fire Conditions</b>		
Ambient temperature (K)	361	Post-fire temperature of 190°F from <i>Discipline Design Guide and Standards for Surface Facilities HVAC Systems</i> Ref. D4.1.16, Section 3.2). This value is 100 °F higher than the maximum interior facility temperature
Heat transfer coefficient (W/m <sup>2</sup> K)	2.0	Natural convection based on anticipated post-fire surface temperature and standard convective heat transfer correlations (Results not sensitive to this value)

NOTE: <sup>a</sup>Composite properties representing both the stainless steel cask wall and depleted uranium gamma shield.  
DU = depleted uranium; SAR = Safety Analysis Report.

Source: Original

Table D2.1-10. Summary of Fuel Failure Probabilities

Fuel Failure Temperature	Monte Carlo Results		Failure Probability	
	Total Failures	Total Trials	Mean	Standard Deviation
700°C	54	100,000	$5.4 \times 10^{-4}$	$7.4 \times 10^{-5}$
750°C	27	100,000	$2.7 \times 10^{-4}$	$5.2 \times 10^{-5}$
800°C	13	100,000	$1.3 \times 10^{-4}$	$3.6 \times 10^{-6}$

Source: Original

#### D2.1.5.4 Analysis to Determine Failure Probabilities for Casks Exposed to Fire

NUREG/CR-6672 (Ref. D4.1.65, Section 6) provides an analysis of seal failure in bare fuel transportation casks. The analysis uses a simple 1-D axisymmetric heat transfer model that is similar to the simple model used in the fire fragility analysis presented in Section D2. The simple model is used to determine the length of time the cask could be exposed to an 800°C or 1,000°C fire before seal failure would be predicted.

The report notes that the elastomer seals used in many transportation casks degrade completely at 500°C, but that the degradation rate increases significantly at 350°C (Ref. D4.1.65, p. 2-9).

Other seal degradation information provided by cask vendors indicates that the maximum design temperature for the metallic o-ring seals in the TN-68 casks is 536°F (280°C) (Ref. D4.1.66, p. 3-2). This is the maximum safe temperature for continuous operation. The actual failure temperature for these seals would be much higher. Based on this information, seal failure is anticipated at temperatures of around 350°C to 450°C.

NUREG/CR-6672 indicates that the seals in a steel/depleted uranium truck cask would reach 350°C if exposed to a 1,000°C fire for 0.59 hours (Ref. D4.1.65, Table 6.5). In a steel/lead/steel (SLS) truck cask, this temperature would be reached in 1.04 hours. The times for rail casks were longer at 1.06 hours for an SLS rail cask and 1.37 hours for a monolithic steel rail cask.

The probability distributions for fire temperature and fire duration discussed in section D2.1.1 can be used to determine the probability that the fire conditions listed in the preceding paragraph would be exceeded. This is accomplished by first determining the probability distribution (using Crystal Ball) for the maximum thermal radiation energy from the fire using the following equation:

$$Q_{\text{rad}} = \sigma A T_{\text{fire}}^4 t_{\text{fire}} \quad (\text{Eq. D-25})$$

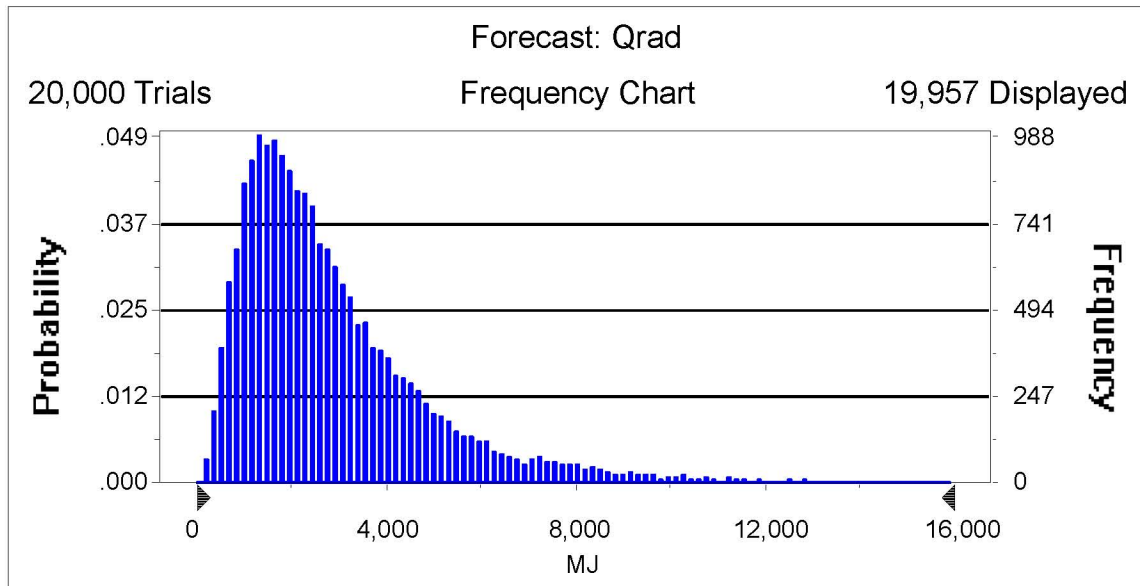
where

- $\sigma$  = the Stefan-Boltzmann constant ( $5.668 \times 10^{-8} \text{ W/m}^2 \text{ K}^4$ )
- $A$  = cask surface area exposed to the fire
- $T_{\text{fire}}$  = fire temperature (sampled from the probability distribution)
- $t_{\text{fire}}$  = fire duration (sampled from the probability distribution)

The probability distribution for  $Q_{\text{rad}}$  is shown in the Figure D2.1-7.

Next, the value for  $Q_{\text{rad}}$  corresponding to the NUREG/CR-6672 (Ref. D4.1.65) fire temperature and duration for seal failure is calculated. The probability distribution for  $Q_{\text{rad}}$  can then be used to determine the probability that the fire will be severe enough to cause seal failure (i.e., will exceed the value for  $Q_{\text{rad}}$  calculated based on the NUREG/CR-6672 conditions).

The values for  $Q_{\text{rad}}$  corresponding to a 1,000°C fire and the fire durations reported in NUREG/CR-6672 (Ref. D4.1.65) are listed below along with the probability of exceedance determined from the probability distribution. The exceedance probabilities can be used as an estimate of the seal failure probability for seals that fail at the temperature,  $T_{\text{fail}}$ , listed in Table D2.1-11. For example, for a SLS truck cask that has seals that fail at 350°C, the probability that the seals fail due to a fire is  $6.9 \times 10^{-3}$ .



Source: Original

Figure D2.1-7. Distribution of Radiation Energy from Fire

By multiplying the highest seal failure probability in Table D2.1-11 (0.05) by the highest probability of fire-induced cladding failure in Table D2.1-11 ( $5.4 \times 10^{-4}$ ), it is shown that the joint conditional probability of a fire that causes additional cladding failure in a truck cask, given a fire, is less than  $3 \times 10^{-5}$ . Because the fire initiating event frequency over the preclosure period of such truck cask fires is less than 1 (see Attachment F for the facilities that contain these, i.e., Wet Handling Facility and Intra-Site Operations), such fires are beyond Category 2 and not analyzed further.

Table D2.1-11. Probabilities that Radiation Input Exceeds Failure Energy for Cask

Cask Type	T <sub>fail</sub> (°C)	Temperature (°C)	Duration (hrs)	Q <sub>rad</sub> (MJ)	P <sub>exceed</sub>
Steel/DU truck cask	350	1,000	0.59	7,208	$5.0 \times 10^{-2}$
Steel/lead/steel truck cask	350	1,000	1.04	12,405	$6.9 \times 10^{-3}$
Steel/lead/steel rail cask	350	1,000	1.06	12,950	$5.6 \times 10^{-3}$
Monolithic steel rail cask	350	1,000	1.37	16,737	$1.7 \times 10^{-3}$
Steel/DU truck cask	500	1,000	≈ 1.0 <sup>a</sup>	≈ 12,200	$7.1 \times 10^{-3}$
Steel/lead/steel truck cask	500	1,000	≈ 1.3 <sup>a</sup>	≈ 15,900	$2.2 \times 10^{-3}$

NOTE: <sup>a</sup>Estimated from Figure 6.6 in NUREG/CR-6672 (Ref. D4.1.65).  
DU = depleted uranium; hrs = hours.

Source: Original

## D2.2 SHIELDING DEGRADATION IN A FIRE

The NUREG/CR-6672 (Ref. D4.1.65) transportation study performed analyses on the internal temperatures of cask for long duration fires of 1,000°C. The transportation study included